Eur. Phys. J. D **31**, 239–262 (2004)
DOI: 10.1140/epjd/e2004-00161-8

THE EUROPEAN PHYSICAL JOURNAL D

Optimizing the photoassociation of cold atoms by use of chirped laser pulses

E. Luc-Koenig[1], M. Vatasescu[1,2], and F. Masnou-Seeuws[1,a]

[1] Laboratoire Aimé Cotton, CNRS, Bâtiment 505, Campus d'Orsay, 91405 Orsay Cedex, France
[2] Institute of Space Sciences, MG-23, 76911 Magurele-Bucharest, Romania

Received 30 June 2004
Published online 23 November 2004 –

Abstract. Photoassociation of ultracold atoms induced by chirped picosecond pulses is analyzed in a non-perturbative treatment by following the wavepacket dynamics on the ground and excited surfaces. The initial state is described by a Boltzmann distribution of stationary continuum states. The chosen example is photoassociation of cesium atoms at temperature $T = 54$ μK from the $a^3\Sigma_u^+(6s, 6s)$ continuum to bound levels in the external well of the $0_g^-(6s + 6p_{3/2})$ potential. We study how the modification of the pulse characteristics (carrier frequency, duration, linear chirp rate and intensity) can enhance the number of photoassociated molecules and suggest ways of optimizing the production of stable molecules.

PACS. 33.80.Ps Optical cooling of molecules; trapping – 33.80.-b Photon interactions with molecules – 33.90.+h Other topics in molecular properties and interactions with photons – 33.80.Gj Diffuse spectra; predissociation, photodissociation

1 Introduction

The various routes leading to the formation of cold and ultracold molecules are actively explored [1]. Non-optical techniques like buffer gas cooling of molecules [2] and Stark deceleration of polar molecules [3,4] reach temperatures well below 1 K. Another route relies on optical techniques, laser fields being used to cool alkali atoms and to create excited molecules via the photoassociation reaction [5]; subsequently, these molecules are stabilized, by spontaneous emission or other radiative coupling, into bound vibrational levels of the ground electronic state [6–11]. The translational temperatures thus reached are much lower ($T \leq 20$ μK). Such long-lived molecules are produced in a superposition of vibrational levels, most of which are very excited. Bringing the molecules to the lower vibrational level ($v = 0$), thus making vibrationally cold molecules, is an important issue [12].

Up to now, most photoassociation experiments are using continuous lasers, but there are a few papers treating the photoassociation with pulsed lasers [13–15]. As for theory, several time-dependent studies of photoassociation in the ultracold regime have been proposed [16–20].

Our aim is to investigate the possibility to control cold molecules formation by use of chirped laser pulses. Indeed, it was shown in other applications that picosecond frequency-swept laser pulses produce more selective excitation and better population transfer than transform-limited pulses with the same bandwidth, due to the mechanism of population inversion by adiabatic sweeping [21–24].

Photoassociation of cold atoms with a chirped laser pulse was first explored theoretically by Vala et al. [18], using a Gaussian packet centered at large interatomic distance ($R \approx 200a_0$) as an initial state to describe the collision of two cesium atoms at the temperature $T = 200$ μK, and showing that a picosecond pulse can achieve a total transfer of population under adiabatic following conditions proposed by Cao, Bardeen, and Wilson [25,26]. However, such an approach cannot work at collision energies close to threshold, and if we are interested in the dynamics at distances small enough to produce in a further step stable cold molecules, because a Gaussian wavepacket does not address the actual shape of the initial continuum state. Indeed, in an ultracold collision of two atoms, the kinetic energy k_BT becomes easily smaller than the interaction potential, and the correct representation of the initial continuum state is a thermal distribution of stationary collisional states. At a given collision energy, the behaviour of a continuum state varies a lot with the interatomic distance: at short and intermediate distances the nodal structure is independent of energy, while at large distances the usual plane wave behaviour is observed. As a consequence, the distance range where the excitation takes

[a] e-mail: francoise.masnou@lac.u-psud.fr

place is of great importance for the photoassociation yield. Therefore, a theoretical treatment of the dynamics at very low temperatures needs a quite precise representation of the initial state.

In a previous theoretical paper [20], we have considered the photoassociation of two cold cesium atoms in their ground state with a picosecond chirped pulse that excites several vibrational levels in the $0_g^-(6s + 6p_{3/2})$ external well. This reaction has been widely studied experimentally with continuous lasers [6], so that the relevant potential curves are well-known. The time-dependent Schrödinger equation corresponding to the two-electronic channels ($a^3\Sigma_u^+(6s + 6s)$ and $0_g^-(6s + 6p_{3/2})$) coupled by the laser field was solved using a propagation method [27]. The use of a Mapped Sine Grid representation [28–30], makes possible numerical calculations taking as the initial state in the photoassociation a delocalized stationary collision state corresponding to a temperature of about 50 μK. The chirped pulse has been designed in view of creating a vibrational wavepacket in the excited state, which, after the pulse, moves to shorter internuclear distances and is focussing at the barrier of the double well potential, thus preparing a good initial state for the stabilization process into low vibrational levels of the $a^3\Sigma_u^+(6s+6s)$ potential. Besides its property of focalization, the specificity of the picosecond chirped pulse analyzed in reference [20] is that it leads to a strong transfer of population inside a spatially limited "photoassociation window", and no transfer outside. Finally, the population transfer to the last vibrational levels of the ground $a^3\Sigma_u^+(6s + 6s)$ state is significant, making stable molecules. We have shown that these results can be interpreted in the framework of a two-state model and in the impulsive limit [31], as an adiabatic population inversion taking place in the "resonance window" swept by the pulse.

In the present work, we consider the same photoassociation reaction, and analyze how the results are modified by acting with various pulses, in order to determine how characteristics like duration, chirp rate and energy influence the photoassociation yield. The results obtained using pulses of different durations (ps, tens and hundreds of picoseconds) and energies, can then be used to explore various regimes of population transfer, nonadiabatic effects, and the eventual limits of the impulsive approximation. Moreover, as our calculations are performed using a very large spatial grid (thousands of a_0), the results account for the threshold effects intervening in this continuum-bound transfer of population which takes place at very low energies and implies a large range of distances.

The paper is organized as follows: in Section 2 we present the two-channel model used for describing the photoassociation reaction with a chirped pulse and discuss the representation of the initial state introduced to study the photoassociation dynamics. Section 3 describes the numerical methods used to perform time-dependent propagation on very large spatial grids. Section 4 discuss the choice of the pulse parameters, and treats specific features of the excitation with a chirped pulse, such as the energy range excited resonantly or not resonantly, and the condition for an "adiabaticity window" during the pulse duration. Section 5 compares the results obtained with pulses differing with respect to duration, energy, and chirp rate. In Section 6 we present calculations of the photoassociation probability from a thermal average over the incident kinetic energies, and we estimate the number of molecules photoassociated per pump pulse. Section 7 presents a discussion on the possible ways for the optimization of the process. Section 8 is the conclusion. The article has three appendix, containing: Appendix A — the energy normalization of the ground state continuum wavefunction calculated in a box; Appendix B — the calculation of the chirp rate in the time domain for focussing the excited vibrational wavepacket at the inner turning point; Appendix C — the overlap of the initial continuum with the 0_g^- vibrational wavefunctions.

2 Two-channel model for the photoassociation with a Gaussian chirped pulse

2.1 The photoassociation reaction

The photoassociation reaction studied here (see Fig. 1) is between two cold cesium atoms colliding in the ground state potential $g \equiv a^3\Sigma_u^+(6s + 6s)$, at a temperature $T \sim 50$ μK, which are excited by a laser pulse to form a molecule in a superposition of vibrational levels $\{v\}$ of the excited electronic potential $e \equiv 0_g^-(6s + 6p_{3/2})$. For a rotational quantum number $J = 0$, it can be represented as:

$$\mathrm{Cs}(6s^2\mathrm{S}_{1/2}) + \mathrm{Cs}(6s^2\mathrm{S}_{1/2}) + \hbar\omega(t) \rightarrow \mathrm{Cs}_2(0_g^-(6s^2\mathrm{S}_{1/2} + 6p^2\mathrm{P}_{3/2}); \{v\}, J = 0). \quad (1)$$

We shall restrict to s wave ($l = 0$), which is a good approximation for cold collisions. For the g and e electronic states, the potentials used in our calculation have been described in a preceding paper [20]. The outer well of the $0_g^-(6s + 6p_{3/2})$ excited potential was fitted to photoassociation spectra by Amiot et al. [32] and matched to ab initio calculations at short and intermediate range [33]. The $a^3\Sigma_u^+(6s, 6s)$ potential has been chosen in order to reproduce correctly the scattering length $L \approx 525a_0$ and the asymptotic behaviour $-C_6/R^6$ with $C_6 = 6828$ au [32] (the short range part extracted from Ref. [34] being slightly modified for that purpose).

We consider the excitation by a chirped laser pulse of Gaussian envelope, having a time-dependent frequency $\omega(t)/2\pi$ which varies linearly around the central frequency $\omega_L/2\pi$ reached at $t = t_P$, and red-detuned by δ_L^{at} relative to the D_2 atomic resonance line:

$$\hbar\omega(t_P) = \hbar\omega_L = \hbar\omega_{at} - \delta_L^{at}. \quad (2)$$

$\hbar\omega_{at}$ is the energy of the atomic transition $6s \rightarrow 6p_{3/2}$. The central frequency of the pulse, $\omega_L/2\pi$, or equivalently the detuning δ_L^{at}, determines the crossing point R_L of the two electronic potentials dressed by the photon with the

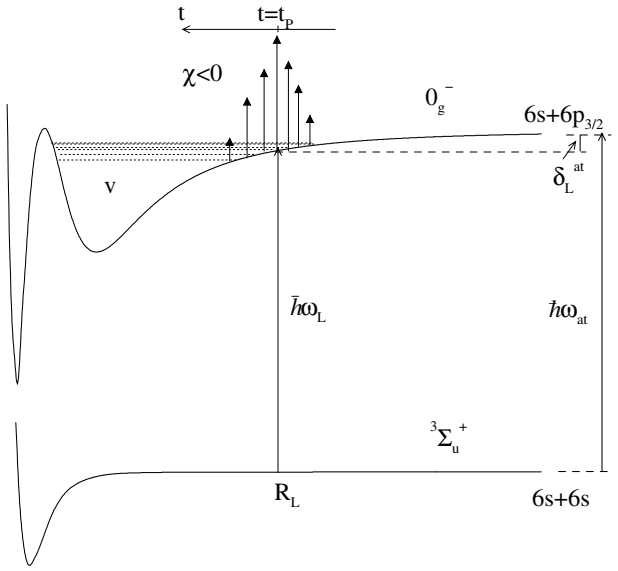

Fig. 1. Scheme of the photoassociation process with a negative chirped pulse considered in the present work, illustrated in the case of Cs_2. The potentials curves correspond to the ground triplet state $a^3\Sigma_u^+(6s+6s)$ and to 0_g^- $(6s+6p_{3/2})$ excited electronic state. In the present work, the energy of the initial continuum state is neglected in the definition of the resonance condition. The double well behaviour in the excited curve is a particular feature of the chosen symmetry.

energy $\hbar\omega_L$ (see Fig. 1). In the present calculations the detuning is fixed at $\delta_L^{at} = 2.656$ cm^{-1}, corresponding to $R_L = 93.7a_0$ and to resonant excitation at the maximum of the pulse of the level $v_0 = 98$ in the external well of the $0_g^-(6s+6p_{3/2})$ potential. In this paper, for the dressed molecule, the origin of energy is chosen at the dissociation limit $(6s+6s)$ of the $a^3\Sigma_u^+$ potential.

2.2 The two-channel coupled equations

We study the dynamics of the photoassociation process in the ground g and excited e electronic states coupled by the electromagnetic field by solving numerically the time-dependent Schrödinger equation describing the wavepacket motion on both surfaces.

The electric field describing a pulse with Gaussian envelope and linear chirp [20,25,26] has the amplitude $\mathcal{E}_0$, a Gaussian envelope $f(t)$, the carrier frequency $\omega_L/2\pi$, and a phase $\varphi(t)$ which is a quadratic function of time:

$$\mathcal{E}(t) = \mathcal{E}_0 f(t)\cos[\omega_L t + \varphi(t)]. \tag{3}$$

The instantaneous frequency $\omega(t)/2\pi$ is given by the derivative of the rapidly oscillating term in $\mathcal{E}(t)$:

$$\omega(t) = \omega_L + \frac{d\varphi}{dt} = \omega_L + \chi(t-t_P), \tag{4}$$

and varies linearly around the central frequency $\omega_L/2\pi$. In equation (4), χ denotes the linear chirp rate in the time domain, equal to the second derivative of $\varphi(t)$. In the dipole approximation, for a pulse with linear polarization $\mathbf{e}_L$, the coupling term between the two electronic channels (g,e) is written as: $-\mathbf{D}_{ge}(R)\cdot\mathbf{e}_L\mathcal{E}(t) \approx D_{ge}^{\mathbf{e}_L}\mathcal{E}(t)$, where $\mathbf{D}_{ge}(R)$ is the R-dependent matrix element of the dipole moment operator between the ground and the excited molecular electronic states. Since the photoassociation reaction occurs at large distances $(R \geq 90a_0)$, we neglect the $R-$dependence, using the asymptotic value $D_{ge}^{\mathbf{e}_L}$ deduced from standard long-range calculations [35].

In the rotating wave approximation with the instantaneous frequency of the chirped pulse, the coupled equations for the radial wavefunctions $e^{\pm i[\omega_L t+\varphi(t)]/2}\Psi_{g,e}^{\omega}(R,t)$ in the ground and excited states can be written as [20]:

$$i\hbar\frac{\partial}{\partial t}\begin{pmatrix}\Psi_e^{\omega}(R,t)\\ \Psi_g^{\omega}(R,t)\end{pmatrix} = \begin{pmatrix}\hat{\mathbf{T}}+\bar{V}(R)+\Delta(R,t) & W_L f(t)\\ W_L f(t) & \hat{\mathbf{T}}+\bar{V}(R)-\Delta(R,t)\end{pmatrix} \times \begin{pmatrix}\Psi_e^{\omega}(R,t)\\ \Psi_g^{\omega}(R,t)\end{pmatrix}. \tag{5}$$

Equation (5) corresponds to a rotating-frame transformation, leading to a "frequency-modulated frame" [24]. The coupling between the two channels writes as:

$$W_L f(t) \leq W_L\sqrt{\frac{\tau_L}{\tau_C}} = W_{max},$$
$$W_L = -\frac{1}{2}\mathcal{E}_0 D_{ge}^{\mathbf{e}_L} = -\frac{1}{2}\sqrt{\frac{2I}{c\epsilon_0}}D_{ge}^{\mathbf{e}_L}. \tag{6}$$

The diagonal terms of the Hamiltonian matrix contain the kinetic energy operator $\hat{\mathbf{T}}$, the mean potential $\bar{V}(R)$:

$$\bar{V}(R) = \frac{V_e(R)+V_g(R)}{2}, \tag{7}$$

($V_g(R)$ and $V_e(R)$ denote respectively the ground and excited electronic potentials) and the R- and t-dependent energy difference $\Delta(R,t)$ between the potentials dressed by the instantaneous laser energy $\hbar\omega(t)$ (defined in Eq. (4)):

$$2\Delta(R,t) = 2\Delta_L(R) - \hbar\frac{d\varphi}{dt} = 2\Delta_L(R) - \hbar\chi(t-t_P), \tag{8}$$

where $2\Delta_L(R)$ is the R-dependent energy difference between the two electronic potentials V_e, V_g dressed by the mean laser energy $\hbar\omega_L$ which are crossing in R_L:

$$2\Delta_L(R) = V_e(R) - V_g(R) - \hbar\omega_L, \tag{9}$$
$$2\Delta_L(R_L) = 0,\ 2\Delta_L(R\to\infty) \to \delta_L^{at}. \tag{10}$$

The instantaneous crossing point $R_C(t)$ between the two dressed potentials is defined by:

$$\Delta(R_C(t),t) = 0;\quad R_C(t_P) = R_L. \tag{11}$$

2.3 Representation of the initial state in the photoassociation dynamics

2.3.1 Thermal equilibrium at temperature T

The initial state of the photoassociation process is chosen to describe a thermal equilibrium state in a gas of cold alkali atoms, lying in a trap of infinite dimension with the laser turned off (then not interacting with the electromagnetic field), and being initially in their ground state. In the present paper the hyperfine structure is neglected. We suppose low atomic densities for which the binary events are isolated enough, such as the Hamiltonian can be reduced to a summation of non-interacting pair Hamiltonians, treated in the Born-Oppenheimer approximation [36]. Then, for a colliding pair of atoms, the molecular Hamiltonian H_M of the relative motion can be separated from the center of mass motion which does not play any role in photoassociation. Assuming thermal equilibrium at temperature T, the initial state is a statistical mixture of eigenstates corresponding to H_M, described by a density operator which can be decomposed into partial waves l.

Restricting our study to s wave, the initial state of the photoassociation process will be described by a density operator $\hat{\rho}_s$:

$$\hat{\rho}_s = \frac{1}{Z}\int_0^\infty dE e^{-\beta E}|E\rangle\langle E| \qquad (12)$$

with $\beta = 1/(k_B T)$, k_B denoting the Boltzmann constant. Here $|E\rangle \equiv |^3\Sigma_u^+, l = 0, E\rangle$ are continuum eigenstates (normalized per unit energy) of the Hamiltonian $\hat{H}_{l=0} = \hat{P}_R^2/2\mu + V_{^3\Sigma_u^+}(R)$ corresponding to the relative motion (R designs the interatomic coordinate and $\hat{P}_R^2/2\mu = \hat{T}$ is the kinetic energy operator) in the electronic potential $V_g(R) = V_{^3\Sigma_u^+}(R)$ and to $l = 0$. $Z = \mathrm{Tr}\{e^{-\beta \hat{H}_M}\}$ is the partition function for a gas composed of non-interacting pairs of atoms in a volume V [37]:

$$Z = Q(T)V, \quad Q(T) = \frac{(2\pi\mu k_B T)^{3/2}}{h^3}, \qquad (13)$$

with μ the reduced mass of the diatom.

The initial state (Eq. (12)) corresponds to an incoherent average, with relative weight $e^{-\beta E}$ over continuum eigenstates $l = 0$ in the ground electronic surface. Such a thermal distribution of collision states has been introduced as initial state in the analysis of the photoassociation of cold Na atoms ($T \sim 0.6$ mK) through wavepacket dynamics [16]. Other authors studying the photoassociation of ultracold Cs atoms ($T \leq 200$ μK) use a Gaussian wavepacket [17,18]. In the following we shall discuss the most suitable representation of the initial state in the study of the photoassociation dynamics by time-dependent propagation calculations. As it will be shown, this choice depends on the detuning δ_L^{qt}, on the temperature T and on the adiabatic character of the population transfer.

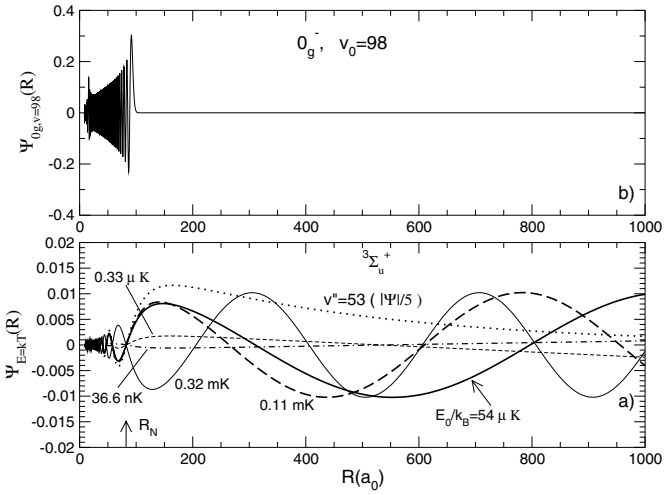

Fig. 2. (a) Stationary continuum states in the $a^3\Sigma_u^+(6s+6s)$ potential, corresponding to energies $E = k_B T$, which are calculated on a grid of length $L_R = 19250a_0$ and normalized at 1 in the box. R_N is the last node common to the collisional wavefunctions in the studied domain of energies. The full thick line represents the continuum wavefunction chosen as initial state in photoassociation at the temperature $E_0/k_B = 54$ μK. Other continuum wavefunctions obtained in the box are represented, corresponding to the following values of E/k_B: 36.6 nK (dot-dashed line), 0.33 μK (short-dashed line), 0.11 mK (long-dashed line), and 0.32 mK (thin continuum line). The last bound state $v'' = 53$ of the triplet potential is also shown (with the wavefunction diminished by a factor of 5); (b) the wavefunction corresponding to the level $v_0 = 98$ in the outer well of the $0_g^-(6s+6p_{3/2})$ potential, which is resonant at $t = t_P$ ($E_{v_0} = -2.656$ cm^{-1} under the dissociation limit $6s + 6p_{3/2}$).

2.3.2 Collisional eigenstates on the $a^3\Sigma_u^+$ surface

Some stationary continuum states $|E\rangle$ with $l = 0$ in the $a^3\Sigma_u^+(6s + 6s)$ potential involved in the description of the initial state (Eq. (12)) are presented in Figure 2a. As discussed in Section 2.3.5, the energy of these scattering states is obtained by quantization in a box with size L_R and the wavefunctions are normalized to unity in this box. Two different behaviours are observed depending on the R-range, leading to different possible descriptions for the initial state.

Until $R_N = 82.3a_0$, which is the position of the last node common to all scattering wavefunctions, all continuum wavefunctions have the same R-dependence and therefore the same nodal structure, the potential energy $V_g(R)$ being larger than the kinetic energy $\hat{T}$. Therefore the initial wavefunction for $R < R_N$ is obtained by solving the stationary Schrödinger equation in the $V_{^3\Sigma_u^+}$ potential. The normalization of this thermal distribution depends on the temperature.

In the range $R > R_N$, each scattering wavefunction with energy E has its specific nodal structure given by the local de Broglie wavelength $h/\sqrt{2\mu[E - V_{^3\Sigma_u^+}(R)]}$. Therefore at large distances $R \gg R_N$ the distribution of continuum states is uniform and at a given temperature

T explicit summation over continuum states $|E\rangle$ has to be evaluated to obtain the density probability of the initial state in a given R-range.

2.3.3 Validity of the description of the initial state by Gaussian wavepackets

When only a narrow R-range located at $R \gg R_N$ contributes significantly to the photoassociation process, an uniformly R-distributed set of localized incoming Gaussian wavepackets can be used to represent the initial state. Each wavepacket has a mean velocity $\bar{v}_0$ equal to the most probable velocity of a Maxwell-Boltzmann distribution (then the corresponding momentum $p_0 = \mu\bar{v}_0 = \sqrt{2\mu k_B T} = \sqrt{\langle p_0^2 \rangle}$, and the momentum spread is defined as $\Delta p_R = p_0/2$). The width ΔR of the radial density distribution of each wavepacket is related to the momentum spread for the relative motion by $\Delta R \Delta p_R \approx \hbar/2$, then depending upon the temperature [18,19].

For a sufficiently small detuning δ_L^{at}, the crossing point R_L of the electronic potentials dressed by the mean laser energy $\hbar\omega_L$ occurs at large distance. For excitation with a continuous laser, the photoassociation process is resonant at R_L, which determines the R-domain governing the dynamics of the process. Then the vibrational level resonantly populated in the 0_g^- surface has its external turning point close to R_L (see Fig. 2 where $R_L \sim R_N$). For the photoassociation with a chirped pulse, other factors such as the duration, the intensity of the pulse and its chirp rate (see Sect. 4.3), strongly influence the distance range which can be excited. As seen in [20] these parameters determine the adiabaticity properties of the population transfer. For sufficiently short pulses for which the impulsive approximation is valid [31] and for adiabatic transfer, only a small R-window located around R_L contributes to the dynamics [20], which strongly reduces in the completely delocalized initial state the effective R-range responsible for the dynamics.

For sufficiently high temperatures T, one can expect that the kinetic energy dominates the interaction potential with behaviour $V_{^3\Sigma_u^+}(R) \sim -C_6/R^6$ at large R distances. The latter condition can be written:

$$k_B T \gg \frac{C_6}{R^6}, \tag{14}$$

resulting in a relatively uniform R-dependence in the wavefunctions $|E\rangle$ which behave as plane waves.

Therefore for a sufficiently small detuning δ_L^{at} and for sufficiently high temperature T, when the laser pulse induces an adiabatic population transfer within a photoassociation window, the dynamics of the photoassociation process can be analyzed by choosing as initial state a single Gaussian wavepacket centered at R_L, if the T-dependent width ΔR of the Gaussian wavepacket is larger than the spatial width of the photoassociation window. With this description of the initial state it is possible to analyze the dynamics of the photoassociation process but the absolute value of the photoassociation rate cannot be calculated.

Gaussian wavepackets have been successfully used in the study of photoassociation with a chirped pulse [18] at a large distance $R_L = 200a_0$ and at the temperature $T = 200$ μK, for a pulse duration (75 ps) sufficiently small to avoid observable motion on the ground surface, but sufficiently large to correspond to a photoassociation window narrower than the width of the Gaussian wavepacket.

On the opposite, in a previous paper [19] studying the photoassociation with a continuous laser in the electronic state $1_g(6s + 6p_{3/2})$ of Cs_2, at $R_L = 90a_0$ and for a temperature $T = 125$ μK, we have shown that a Gaussian wavepacket having a large radial width and a small momentum p_0 is spreading more rapidly than it is moving; since it was quite difficult to gain insight on the relevant dynamics by using it, a possible choice was to consider a much smaller spatial width, implying a bigger momentum spread. Components with much bigger momenta are then introduced in the representation of the initial state, falsifying the dynamics in the corresponding channel.

2.3.4 Evaluation of the initial density matrix by stationary collisional eigenstates

In the case of the $a^3\Sigma_u^+(6s + 6s)$ state of Cs_2, for the temperature $T \approx 50$ μK studied in the present paper, the relation (14) is valid for $R \gg 185a_0$, which corresponds to resonant excitation of vibrational states with $v \gg 130$ in the $0_g^-(6s + 6p_{3/2})$ external well, or to a laser detuning $\delta_L^{at} \ll 0.35$ cm^{-1}. At $T \approx 50$ μK (a collision with relative velocity $\bar{v}_0 \approx 10$ cm/s), the width corresponding to a radial wavepacket is very large: $\Delta R \approx 160a_0$ (in cold collisions the large de Broglie wavelength describing the relative motion is the sign of the wavefunction delocalization). Therefore at $T \sim 50$ μK the representation of the initial state by Gaussian wavepackets cannot be used if we are interested in the real dynamics at small distances and in the initial molecular channel, because it hardly addresses properly the physics at distances different from R_L. Then it is absolutely necessary to account for the nodal structure of the ground state wavefunction, which is responsible for the intensity minima observed in the photoassociation spectra [1].

This is the case for the example studied in the present paper which concerns the photoassociation in the $0_g^-(6s + 6p_{3/2})$ channel in Cs_2, at a detuning $\delta_L^{at} \approx 2.4$ cm^{-1}, $R_L \approx 94a_0$, and $T \approx 50$ μK. Indeed, in this case $R_L \sim R_N$ (see Fig. 2), and it is necessary to describe the initial state as an incoherent average over a thermal distribution of stationary energy-normalized continuum wavefunctions $|E\rangle$, as in equation (12). Several time-propagation calculations are performed, each using a particular initial state $|E\rangle$ of the thermal energy distribution and corresponding to a density probability $|\Psi_{0_g^-}^E(R,t)|^2$ transferred at the time t in the 0_g^- surface. Then the total density probability corresponding to the thermal distribution at temperature T is obtained from the incoherent average: $(1/Z)\int_0^\infty e^{-\beta E}|\Psi_{0_g^-}^E(R,t)|^2 dE$ (see Eq. (34) in Sect. 6). In the present work we begin by performing time-dependent

photoassociation calculations taking as initial state a single continuum state $|E_0\rangle$ of the thermal energy distribution (Sect. 5); next, the photoassociation probability is calculated as a thermal average over the incident kinetic energies (Sect. 6) leading to an estimation for the absolute value of the photoassociation rate.

2.3.5 Discretization and energy-normalization of the scattering spectrum

In our method, the eigenstates of the Hamiltonian associated with the ground electronic channel are calculated through the Sine Grid Representation [28–30], in a large box of radius L_R which introduces a discretization of the continuum (only continuum states having a node at the boundary of the box are obtained) and supplies wavefunctions normalized to unity in the box. We shall label $E_n > 0$ the energies of these states and $\phi_{E_n}(R)$ the corresponding wavefunctions having n nodes in the range $R_N < R < L_R$ ($n \geq 0$ integer). The energy resolution in a box of length L_R is determined by the energy difference δE corresponding to neighbouring eigenstates of the box:

$$\delta E\ |_{E_n} = \frac{\partial E}{\partial n}\ |_{E=E_n} = \frac{\hbar\pi}{L_R}\sqrt{\frac{2E_n}{\mu}} = \frac{\hbar^2\pi^2}{\mu L_R^2}n. \qquad (15)$$

Then a large box is necessary to have a sufficiently high energy resolution (small δE), able to represent low energies corresponding to the temperature $T \approx 50$ μK. For the present calculations we use a box with the width $L_R = 19250a_0$, in which the continuum state having the energy $E_n = k_B T$, with $T = 54$ μK, is the 38th state in the corresponding discretized continuum. This leads to a resolution at threshold $\delta E/k_B = 30$ nK and $(1/k_B)(\partial E/\partial n)\ |_{E/k_B=54\ \mu\mathrm{K}} = 2.6$ μK for the continuum description around 54 μK. Such a large box allows to account correctly for the threshold behaviour in the cold collision process and to perform explicitly an average on the thermal energy distribution (see Sect. 6).

For an energy resolution δE, the maximum relevant time scale which can be studied in the problem is $\tau_{max} = \hbar/\delta E$. Any energy spacing smaller than δE is not resolvable in the box of length L_R (for example, an eigenstate characterized by a vibrational period bigger than τ_{max} cannot be distinguished from the continuum positive energy states in the box determined by this L_R). In the present case τ_{max} is 2.9 μs, being larger than the radiative lifetime in the 0_g^- state, $\tau_{rad} \approx 15$ ns; but the spontaneous emission is not introduced in the present problem, where the dynamics is followed for times smaller than τ_{rad}.

The representation of the initial density matrix by stationary continuum states needs a normalization per unit energy of the continuum wavefunctions. The basic formulae are shown in the Appendix A: one shows that the relation between the wavefunctions $\Psi_{E_n}(R)$ normalized per unit energy and the wavefunctions $\phi_{E_n}(R)$ normalized to unity in the box is the following:

$$\Psi_{E=E_n}(R) = \left[\frac{\partial E}{\partial n}\ |_{E=E_n}\right]^{-1/2} \phi_{E_n}(R). \qquad (16)$$

In the present Grid representation the density of states is calculated explicitly from the energy spacing between two neighbouring states of the discretized continuum:

$$\frac{\partial E}{\partial n}\ |_{E=E_n} = E_{n+1} - E_n. \qquad (17)$$

3 Numerical methods

The dynamics of the photoassociation process is performed by numerical solution of the time-dependent Schrödinger equation (5) for the ground $V_g(R)$ and excited $V_e(R)$ potentials coupled by the electromagnetic field, taking as initial state $\Psi_g(R,0)$ a stationary continuum state of the ground surface of very low energy $E = k_B T$, corresponding to a temperature $T = 54$ μK. A grid of very large extension is needed to represent correctly such an initial state and the last bound states of the ground potential which are populated during the photoassociation process, and whose wavefunctions extend at large interatomic distances. We consider a grid extending from L_0 (a distance slightly smaller than the repulsive walls in the potentials, here $L_0 = 8a_0$) to $L_R = 19250a_0$ in the present paper. This very large grid allows to represent correctly the wavefunctions implied in the process and to account for the threshold behaviours at low energies in the realistic potentials.

3.1 Spatial representation of the wavefunctions

The radial dependence of the wavepackets $\Psi_{e,g}(R,t)$ propagating on both surfaces is represented using Mapped Grid Methods [29,30]. The mapping works with a change of variable (from R to the adaptive coordinate x) taking account of the variation of the local de Broglie wavelength $\Lambda(E,R) = h/\sqrt{2\mu[E - V_g(R)]} = 2\pi\hbar/p_R$ as a function of the internuclear distance R. Namely, the Jacobian of the transformation is chosen proportional to the local de Broglie wavelength: $J(x) = dR/dx = \beta\Lambda(E_{max}, R)$, where E_{max} is the maximum energy involved in the problem. This leads to the implementation of a large spatial grid by using only a small number of points. For example, in our calculations we use $N = 1023$ points for a spatial extension $L_R = 19250a_0$, uniformly describing regions of space where $\Lambda(E_{max}, R)$ varies by several orders of magnitude. The use of an enveloping potential $V_{env}(R)$ (equal to or deeper than the crossing V_e and V_g potentials dressed by the field) allows the definition of a common Jacobian and therefore a single x-grid to describe both surfaces. In the new coordinate x, the kinetic energy operator is expressed simply as product of operators $J(x)^{-1/2}$ and d/dx, improving the numerical accuracy [29,30]. The potential energy operator reduces simply to $V(x)$.

A collocation method [29,30] is used to define the representation of the wavefunctions in the N points x_i of the grid (x). This supposes that any wavefunction $\bar{\Psi}(x)$ is expanded on a set of N basis functions. Instead of the usual plane wave expansion (Fourier expansion),

we use the Sine expansion recently introduced by Willner et al. [30]. All basis sine functions have nodes at the boundaries L_0 and L_R of the grid, which, by choosing a sufficiently small β-value [30], permits the suppression of the so-called "ghost" levels appearing in the solution of the stationary Schrödinger equation and then susceptible to falsify the dynamics of the system. We have verified that a value $\beta = 0.52$ is necessary for avoiding the appearance of "ghost" levels.

To determine the stationary eigenstates of the ground or excited potential (which are used either for the selection of the initial state, or to analyze the wavepackets evolution in terms of their decompositions on stationary states) an auxiliary cosine basis set is introduced, allowing to evaluate analytically the first order derivatives d/dx involved in the kinetic energy operator [30].

In time propagation calculations one has to multiply repeatedly the initial state wavefunction by the Hamiltonian matrix. Therefore one has to express the kinetic energy operator in terms of discrete sine and cosine Fourier transformations [38], for which we use the efficient fast Fourier algorithms. This imposes $N = 2^p - 1$ (p integer) for the number of grid points ($N = 1023$ for the present calculation).

Lastly, in time propagation calculations the initial state is normalized to unit in the box of size L_R. Therefore the populations $P_{0_g^-}(t)$ or $P_{^3\Sigma_u^+}(t)$ calculated at a time t are depending on the value chosen for L_R. Nevertheless, due to the normalization condition $P_{0_g^-}(t) + P_{^3\Sigma_u^+}(t) = 1$, which is verified for every t, the calculations give directly the relative population on each surface.

3.2 Time evolution

The time-dependent Schrödinger equation for the two coupled channels (see Eq. (5)) is solved by propagating the initial wavefunction using a Chebychev expansion of the evolution operator $\exp[-i\hat{\mathbf{H}}t/\hbar]$ [27,28]. Propagation is performed in discrete steps with a time increase Δt much shorter than the characteristic times of the problem (pulse duration, vibrational periods, Rabi periods). In the present study of photoassociation with chirped pulses the Hamiltonian $H(t)$ is explicitly time-dependent, and a discrete description of $H(t)$ is introduced. During the step corresponding to time propagation from t_1 to $t_2 = t_1 + \Delta t$, the Hamiltonian is supposed to be time-independent and chosen as $H(t_m)$, where $t_m = (t_1 + t_2)/2$. Such a procedure introduces errors of the order of magnitude $(\Delta t)^3$. Since presently the initial state is a stationary collisional eigenstate in the $^3\Sigma_u^+$ potential, instead of a Gaussian wavepacket, the dynamics results only from coupling with the laser pulse, but not from the motion characteristic of the evolution of a nonstationary state. Moreover, the dynamics is studied within a very large box. Consequently, even after a very long propagation duration of 15 ns (the order of magnitude of the spontaneous emission time for the vibrational levels excited in the 0_g^- state), the wavepackets dynamics in the range of distances relevant for our problem (in which the hyperfine structure is neglected) is not influenced by the external boundary of the box. Therefore there is no reflection of the wavepackets at L_R and then it is not necessary to define outgoing wave boundary conditions for the wavepackets (either by transferring the outgoing part to another grid [39] or by introducing an imaginary absorbing potential [40]).

In the present problem, using a grid with $N = 1023$ points, which for $\beta = 0.52$ gives a box of extension $L_R = 19250a_0$, the energy resolution at the $^3\Sigma_u^+$ dissociation threshold is determined by $\delta E/k_B \approx 100$ nK. For a grid with only 511 points, the extension is reduced by a factor of about 7.8 and the energy resolution is strongly diminished, as $\delta E/k_B \approx 6$ μK. Since we study the photoassociation taking an initial stationary state corresponding to $T \approx 50$ μK, a grid of large extension is needed to reach the necessary resolution in the representation of the threshold processes. As we have shown before, this is possible due to the mapping procedure, which drastically reduces the number of grid points, and to the implementation of the Sine Basis representation, which eliminates the participation of the "ghost levels" in the dynamics.

For the step-size $\Delta t \approx 0.05$ ps used in our time propagation, $\hat{\mathbf{H}}\Psi$ is calculated 112 times during each interval Δt. Therefore the implementation of the fast Fourier transformations to calculate $\hat{T}\Psi$ avoids prohibitive calculation times, allowing in principle to study the evolution of the wavepackets during time durations as long as 10 ns (which corresponds to a repetition rate of 10^8 Hz for the photoassociating laser pulse). Obviously, such long evolution times need to introduce in the problem other physical processes, such as the spontaneous emission ($\tau_{rad} = 15$ ns), which is not taken into account in the present calculations.

4 Excitation with chirped pulses: optimizing the pulse

4.1 Parameters for Gaussian pulses with linear chirp

We consider pulses with Gaussian envelope and linear chirp, as discussed in references [20,25,26]. Since both the amplitude and the frequency of the electric field $\mathcal{E}(t)$ defined in equation (3) are time-dependent, the pulses are characterized by various parameters that should be optimized. The first parameter τ_C characterizes the temporal width of the Gaussian envelope $f(t)$ in the amplitude $\mathcal{E}(t)$ (Eq. (3)):

$$f(t) = \sqrt{\frac{\tau_L}{\tau_C}} \exp\left[-2\ln 2\left(\frac{t - t_P}{\tau_C}\right)^2\right], \qquad (18)$$

which is maximum at $t = t_P$ and has the full width at half maximum (FWHM) equal to $\sqrt{2}\tau_C$.

Next, the duration τ_L characterizes the spectral width $\delta\omega = 4\ln 2/\tau_L$ in the frequency domain: indeed, $\tilde{\mathcal{E}}(\omega)$, which is the Fourier transform of $\mathcal{E}(t)$, displays a Gaussian profile with FWHM equal to $\sqrt{2}\delta\omega$.

The ratio τ_C/τ_L characterizes the chirp. The linear chirp is determined by the chirp rates: χ in the time domain (calculated as the second derivative of the phase $\varphi(t)$

of the field $\mathcal{E}(t)$, see Eq. (3)), and Φ'' in the frequency domain (the second derivative of the phase of $\tilde{\mathcal{E}}(\omega)$), so that the ratio τ_C/τ_L reads:

$$\frac{\tau_C}{\tau_L} = \sqrt{1 + (4\ln 2)^2 \frac{(\Phi'')^2}{\tau_L^4}} = \sqrt{1 + \frac{\chi^2 \tau_C^4}{(4\ln 2)^2}}. \qquad (19)$$

The condition $\tau_C = \tau_L$ corresponds to an unchirped transform-limited pulse with duration τ_L, and in the general case the duration is stretched to τ_C by chirping, so that $\tau_C/\tau_L \geq 1$. The choice of τ_L and χ determines the pulse duration τ_C (see Eq. (19)), and then the chirp rate in the frequency domain:

$$\Phi'' = \chi \frac{\tau_C^2 \tau_L^2}{(4\ln 2)^2} \qquad (20)$$

with two possible values for both quantities, as discussed below in Section 4.2. Among the four parameters τ_C, τ_L, χ and Φ'', only two are independent (see Eqs. (19) and (20)).

Another independent parameter is the coupling W_L defined in equation (6), depending upon the intensity I_L and the dipole transition moment. Chirping a pulse increases its duration and decreases its maximum amplitude: $\mathcal{E}_M = \mathcal{E}_0\sqrt{\tau_L/\tau_C} \leq \mathcal{E}_0$. As a result, the chirp does not change the energy E_{pulse} carried by the field, which is proportional to the square of the amplitude $\mathcal{E}_0$ and to the temporal width τ_L of the transform limited pulse: $E_{pulse} = (c\epsilon_0/2)\int_{-\infty}^{+\infty} |\mathcal{E}(t)|^2 dt = (I_L\tau_L/2)\sqrt{\pi/\ln 2}$, with $I_L = (c\epsilon_0/2)/\mathcal{E}_0^2$ (c is the velocity of light and ϵ_0 the vacuum permittivity).

Therefore, for a given central frequency ω_L, the choice of three independent parameters (W_L, and two of the four parameters discussed above) will determine the main properties of the pulse and in particular the adiabatic character of the population transfer.

4.2 The choice of the chirped pulse parameters

There are many possibilities for the design of chirped pulses, and their choice will depend upon the objective of a given experiment. In the present paper, our choice is to fix the carrier frequency $\omega_L/2\pi$ (or, equivalently, the detuning δ_L^{at}), the coupling W_L (or the intensity I_L), and the chirp rate χ in the time domain. On the other hand, we shall study pulses of different durations τ_L (or various spectral widths $\delta\omega$), leading to different situations for the energy range $2\hbar|\chi|\tau_C$ (see Ref. [20]) swept by the central frequency, for the maximum $W_{max} = W_L\sqrt{\tau_L/\tau_C}$ of the coupling, and for the energy of the pulse E_{pulse} (proportional to $W_L^2\tau_L$). Our choice to keep W_L constant differs from experimental situations where it is easier to keep E_{pulse} constant, shorter pulses having larger maximal intensity. Fixing the coupling W_L, instead of E_{pulse}, leads to situations as various as possible for either the photoassociation yield or the dynamics of the process. Indeed, the pulses which are studied induce quite different excitation regimes, due to their characteristics: narrow or broad bandwidth $\delta\omega$, short or long duration τ_C, small or large chirp Φ'' inducing various ratios τ_L/τ_C and various energies E_{pulse}.

The objective of this work is to analyze the properties of the photoassociated wavepacket as a function of the pulse. We shall study the photoassociation yield and the radial distribution of population transferred in the 0_g^- surface at the end of the pulse, but also the evolution of the wavepackets after the pulse (vibration in the 0_g^- potential and acceleration to the inner region). An important goal is to gain information about the degree of coherent control in the photoassociation process: for example we are interested to maximize the population localized at small distances in the 0_g^- potential (internuclear distances more favorable to radiative stabilization of the photoassociated molecules, by spontaneous or stimulated emission, towards the ground potential surface).

• *Detuning.* We present here calculations for photoassociation with different pulses at the same detuning $\delta_L^{at} = 2.656$ cm^{-1}, corresponding to a crossing point $R_L = 93.7a_0$. The detuning is chosen such as $\delta_L^{at} = E_{v_0}$, the binding energy of the $v_0 = 98$ level in the external well of the $0_g^-(6s + 6p_{3/2})$ potential, which means that at $t = t_P$ there is a resonance condition between the continuum state lying at threshold ($E = 0$) and this vibrational level. Taking into account that the initial collisional state considered here corresponds to a very low temperature $T = 54$ μK, and to an energy $E_0 = k_BT$ much smaller than the vibrational energy spacing in the $0_g^-(6s + 6p_{3/2})$ potential ($(E_{v_0} - E_{v_0-1})/E_0 \approx 3300$), the initial state E_0 is in resonance with the v_0 vibrational level.

• *Intensity I_L and Coupling W_L.* Also, we consider the same laser intensity I_L and then the same coupling W_L for all the pulses. But the pulses with different durations τ_L correspond to different energies $E_{pulse} \sim I_L\tau_L$. For laser excitation with π polarization between the electronic states $^3\Sigma_u^+(6s, 6s)$ and $0_g^-(6s + 6p_{3/2})$, and neglecting the R-variation of the dipole coupling, the intensity is related to the coupling W_L by equation (6), giving W_L (a.u.) $= 9.74 \times 10^{-9}\sqrt{I_L(\mathrm{W/cm^2})}$ [35]. In the present calculations the laser intensity is $I_L = 120$ kW cm^{-2}, giving a coupling $W_L = 0.7396$ cm^{-1}. By chirping the pulse, the instantaneous coupling becomes $W(t) = W_L f(t) \leq W_{max}$.

• *Chirp rate χ in the time domain. Focussing.* The linear chirp parameter χ has been designed in order to achieve, at a time $t = t_P + T_{vib}(v_0)/2$ (where $T_{vib}(v_0)/2 = 125$ ps is half the vibrational period of the level $v_0 = 98$), the focussing of the excited vibrational wavepacket at the internal turning point of the vibrational state v_0 in the 0_g^- outer well. The chirp parameter necessary to compensate the dispersion in the vibrational period of the wavepacket is chosen as $\chi = -2\pi T_{rev}(v_0)/[T_{vib}(v_0)]^3$, i.e. adjusted to match the revival period T_{rev} (see Appendix B) of the resonant level $v_0 = 98$. This leads to $\chi = -4.79 \times 10^{-3}$ ps^{-2} $= -0.28 \times 10^{-11}$ au, and $\hbar\chi = -0.025$ cm^{-1} ps^{-1}.

Table 1. Parameters of Gaussian pulses considered in this work, linearly chirped with the same rate χ in the time domain, and corresponding to the laser intensity at $t = t_P$ for the transform limited pulse $I_L = 120$ kW cm^{-2}, which, for a linear polarization of the electric field, gives a coupling $W_L = 0.7396$ cm^{-1} for the $a^3\Sigma_u^+(6s, 6s) \rightarrow 0_g^-(6s, 6p_{3/2})$ transition at large interatomic distances. The central frequency of the pulse, $\omega_L/2\pi$, resonantly excites the $v_0 = 98$ level of the $0_g^-(6s, 6p_{3/2})$ outer well, with binding energy $E_{v_0} = 2.656$ cm^{-1} and vibrational period $T_{vib}(v_0) = 250$ ps. The significant parameters listed below are: temporal width τ_L of the initial pulse before chirping, spectral width $\hbar\delta\omega$, chirp rate Φ'' in the frequency domain, temporal width τ_C of the chirped pulse, the ratio $\sqrt{\tau_L/\tau_C}$, the chirp rate χ in the time domain, the energy range $\hbar|\chi|\tau_C$ resonantly swept by the pulse during the period $[-\tau_C, \tau_C]$, the maximum coupling $W_{max} = W_L\sqrt{\tau_L/\tau_C} = W(t_P)$, and the parameter α_{max} indicating a limit for the adiabaticity range $[-\alpha\tau_C, \alpha\tau_C]$ ($\alpha \ll \alpha_{max}$). The probability of photoassociation in the 0_g^- surface at the end of the pulse (corresponding to a total population normalized at 1 on the grid), noted $P_{0_g^-}(E_0)$, is also shown (E_0 is the energy of the initial continuum state, $E_0/k_B = 54$ μK). In a trap of volume $V = 10^{-3}$ cm^3, containing 10^8 atoms at the temperature $T = 50$ μK, the number of molecules photoassociated per pump pulse $\mathcal{N}$ is related to $P_{0_g^-}(E_0)$ by: $\mathcal{N} \sim 2000 P_{0_g^-}(E_0)$. The characteristics of the chirped pulse studied in reference [20] are reported in the last line.

	$\hbar\delta\omega$ (cm^{-1})	Φ'' (ps^2)	τ_C (ps)	$\sqrt{\frac{\tau_L}{\tau_C}}$	χ (ps^{-2})	$\hbar\lvert\chi\rvert\tau_C$ (cm^{-1})	W_{max} (cm^{-1})	α_{max}	$P_{0_g^-}(E_0)$
$\tau_L =$ **1 ps**	14.72	−0.00063	**1.002**	0.999	-4.79×10^{-3}	0.025	0.739	1.12	3.961×10^{-2}
		−208.8	**581**	0.042		14.52	0.031	–	3.941×10^{-2}
$\tau_L =$ **6 ps**	2.453	−0.81	**6.012**	0.999	-4.79×10^{-3}	0.15	0.739	1.12	2.168×10^{-2}
		−207.99	**96.28**	0.249		2.41	0.184	0.5	6.005×10^{-2}
$\tau_L =$ **12 ps**	1.227	−13.84	**12.41**	0.983	-4.79×10^{-3}	0.31	0.727	1.11	3.046×10^{-4}
		−194.96	**46.6**	0.507		1.17	0.375	0.87	5.340×10^{-4}
$\tau_L =$ **15 ps**	0.981	−38.51	**16.60**	0.950	-4.79×10^{-3}	0.42	0.703	1.10	1.200×10^{-4}
		−170.00	**34.8**	0.657		0.87	0.486	0.95	3.245×10^{-4}

• *Pulse duration* τ_C. τ_L and χ being chosen, τ_C^2 is solution of the second order equation:

$$\tau_C^4 - \frac{(4\ln 2)^2}{\chi^2\tau_L^2}\tau_C^2 + \frac{(4\ln 2)^2}{\chi^2} = 0 \qquad (21)$$

which gives, as for Φ'', two values of the pulse duration τ_C for a given pair (τ_L, χ). In fact, with the relation (20) one can see that the chirp rate in the frequency domain Φ'' is then determined; pulses with the longer duration τ_C correspond to the higher rate Φ'' in the frequency domain.

• *Temporal width* τ_L *of the pulse before chirping.* Equation (21) shows that the existence of real values of Φ'' and τ_C requires:

$$\tau_L \leq \sqrt{\frac{2\ln 2}{|\chi|}}, \qquad (22)$$

imposing an *upper limit* for the value of τ_L which can still be chosen for a fixed value of χ. On the other hand, one can choose to avoid the excitation of the 0_g^- continuum during the photoassociation process. Such a requirement is related to a *lower limit* for the initial temporal width τ_L, the spectral width of the pulse having to be smaller than the detuning δ_L^{at}:

$$\hbar\delta\omega = \hbar\frac{4\ln 2}{\tau_L} < \delta_L^{at} \Longrightarrow \tau_L > \hbar\frac{4\ln 2}{\delta_L^{at}}. \qquad (23)$$

For the detuning $\delta_L^{at} = 2.656$ cm^{-1} and the chirp rate $\chi = -4.79\times10^{-3}$ ps^{-2} leading to focussing, the conditions (22) and (23) give the following interval of choice for τ_L:

$$5.54 \text{ ps} < \tau_L \leq 17 \text{ ps}, \qquad (24)$$

corresponding to predominant excitation of bound vibrational levels 0_g^-.

For $0 < \tau_L < 5.54$ ps, continuum states of 0_g^- localized at large distances are mainly excited. Let us remark that the border between excitation of bound or continuum states is not well defined, it only corresponds to the FWHM of the spectral energy distribution, without taking into account the absolute intensity of the pulse. In the interval described by the relation (24), the excitation of continuum will become important for an increasing intensity I_L. The characteristics of the pulses studied in the present paper are reported in Table 1, which also shows those of the pulse studied in reference [20].

4.3 The energy range corresponding to a large population transfer induced by the chirped pulse

The impulsive approximation [20,31] can be used to qualitatively determine the spatial range in which the population transfer from the ground to the excited surface is important. Let's take the example of a two-level system with energy splitting $\hbar\omega_{eg} = \hbar(\omega_e - \omega_g)$ which is excited by a pulse characterized by a spectral energy distribution $|\tilde{\mathcal{E}}(\omega)|^2$ (centered on the mean laser pulsation ω_L, FWHM $\delta\omega$, and maximum proportional to the laser intensity I). Longtime after the end of the pulse, and in the perturbative approximation, the population in the excited level is given by $\mu_{ge}^2|\tilde{\mathcal{E}}(\omega_{eg})|^2$, where μ_{ge} is the dipole moment of the transition. Therefore this population grows up when μ_{ge} or I increase and when the detuning $\omega_{eg} - \omega_L$ decreases, being maximum at the resonance ($\omega_{eg} = \omega_L$).

Similar considerations apply for population transfer from the ground to the excited surface; it is favoured: (i) at resonance (i.e. at the instantaneous crossing point $R_c(t)$), (ii) for a large overlap integral $|\langle {}^3\Sigma_u^+ E_0 | 0_g^- v\rangle|^2$ between the initial collisional wavefunction and the resonantly excited vibrational level v having its outer turning point close to $R_c(t)$, and (iii) for large laser intensities.

For a Gaussian pulse, 98% of the energy is carried during the time interval $[-\tau_C, +\tau_C]$, and then the effect of the pulse can be estimated by analyzing it during this *temporal window* [20]. During this time interval, the instantaneous crossing point $R_C(t)$ defined by the relation (11) varies in time, describing a *resonance window*; the energy range resonantly swept by the pulse around the central frequency $\omega_L/2\pi$ is $2\hbar|\chi|\tau_C$, which is limited by its spectral width [20]. Indeed, $|\chi|\tau_C \leq \delta\omega$, with a ratio depending on the chirp rates:

$$\frac{|\chi|\tau_C}{\delta\omega} = \sqrt{\Phi''\chi} = \sqrt{1 - \left(\frac{\tau_L}{\tau_C}\right)^2} \leq 1. \qquad (25)$$

Then, vibrational levels lying in the "resonance window" will be excited by the pulse at different times.

Besides, the large overlap of the initial continuum wavefunction with the 0_g^- vibrational wavefunctions of levels close to the dissociation limit is especially favorable to population transfer at very large distances. Indeed, the overlap integral has a large maximum for vibrational levels having outer turning points at large distances R, close to the dissociation limit (see Appendix C, Fig. 12).

Furthermore, for a large laser intensity, off-resonant excitation can easily become efficient. This is particularly true for cold photoassociation at small detunings if the coupling and detuning have comparable values, leading to noticeable excitation outside the resonance window.

Then, it is interesting to note that using a chirped pulse for such free-bound transitions close to the dissociation limit, it is possible to control the excited energy range by the pulse characteristics, in order to avoid the population of the continuum or to restrain the spatial range covered by the final 0_g^- packet. Indeed, in addition to the spectral width $\delta\omega$ (determined by τ_L for both transform limited or chirped pulses), one can select the range of the window $|\chi|\tau_C$ to be excited resonantly, by choosing the chirp parameters Φ'', χ, or, equivalently, the ratio τ_L/τ_C (see Eq. (25)).

Lastly, the pulse intensity I_L will determine the adiabatic or non-adiabatic character of the transfer (this will be detailed in Sect. 4.4), and the importance of the off-resonance excitation. Nevertheless, the estimated boundary between resonant and off-resonant excitation remains approximative.

4.4 Condition for an "adiabaticity window" during the pulse duration

Efficient adiabatic population inversion can be obtained by using a chirped laser pulse, which in a two state system allows to sweep the instantaneous frequency $\omega(t)$ from far above (respectively far below) to far below (respectively far above) resonance. Sufficiently slow sweeping induces total adiabatic transfer from one state to the other one [20,24–26].

In a previous work [20] we have analyzed adiabatic population inversion within the impulsive limit [31], assuming that the relative motion of the two nuclei is frozen during the laser interaction, i.e. $\tau_C \ll T_{vib}(v_0)$, where $T_{vib}(v_0) = 250$ ps is the vibrational period of the 0_g^- level resonantly populated at $t = t_P$. By neglecting the kinetic energy operator appearing in the two-level Hamiltonian of equation (5), one can introduce a coordinate-dependent two-level model able to define the conditions for full adiabatic population transfer. At the instantaneous crossing points $R_C(t)$, the nonadiabatic effects can be explored using the adiabaticity condition, which in these points takes a simple form determined by the pulse shape ($|\chi|$ and τ_C/τ_L) and its intensity (I_L or W_L) [20]:

$$\hbar^2|\chi| \ll 8(W(t))^2. \qquad (26)$$

The condition (26) will not be verified when $W(t)$ becomes very small. Then, it is useful to estimate the domain $[-\alpha\tau_C, \alpha\tau_C]$, with $\alpha > 0$, for which the adiabaticity condition (26) is verified. For $|t - t_P| < \alpha\tau_C$, the coupling $W(t)$ has the lower bound $W_{max}/4^{\alpha^2}$, so α can be deduced from the condition:

$$\frac{16^{\alpha^2}}{8}\hbar^2|\chi|\frac{\tau_C}{\tau_L} \ll W_L^2, \qquad (27)$$

giving:

$$\alpha \ll \sqrt{\frac{1}{\ln 16}\ln\left\{8\frac{1}{\hbar^2|\chi|}W_L^2\frac{\tau_L}{\tau_C}\right\}} = \alpha_{max}. \qquad (28)$$

For $\alpha \ll \alpha_{max}$, the adiabaticity condition (27) is very well satisfied during all the time interval $[-\alpha\tau_C, \alpha\tau_C]$. For $\alpha \approx \alpha_{max}$, the transfer can be adiabatic during a certain portion of this interval, but strong non-adiabatic effects appear at the boundary $|t - t_P| \approx \alpha_{max}\tau_C$. For $8(1/\hbar^2|\chi|)W_L^2(\tau_L/\tau_C) < 1$ (small intensity I_L and/or large chirp $|\chi|\tau_C/\tau_L$), adiabaticity never occurs, α_{max} not being defined. The values α_{max} corresponding to the pulses studied here are given in the table.

For a given pulse, α_{max} offers an approximate evaluation for the extension of the time interval $[-\alpha\tau_C, \alpha\tau_C]$, with $\alpha \ll \alpha_{max}$, during which the adiabaticity condition can be verified at the instantaneous crossing points. For fixed $|\chi|$ and W_L, it is the ratio τ_L/τ_C which fixes the time-interval during which crossing of the two potentials can lead to population inversion due to adiabatic passage. Then, in the "window" $[R_{min}, R_{max}]$ swept by the instantaneous crossing point, total population inversion occurs. In addition, if, at large distances, the two dressed potential curves do not cross and the dynamics is adiabatic during the time interval $[-\alpha\tau_C, \alpha\tau_C]$, no population transfer occurs. As a result, population transfer occurs only in the range $[R_{min}, R_{max}]$ defining an "adiabaticity window" [20,24,26].

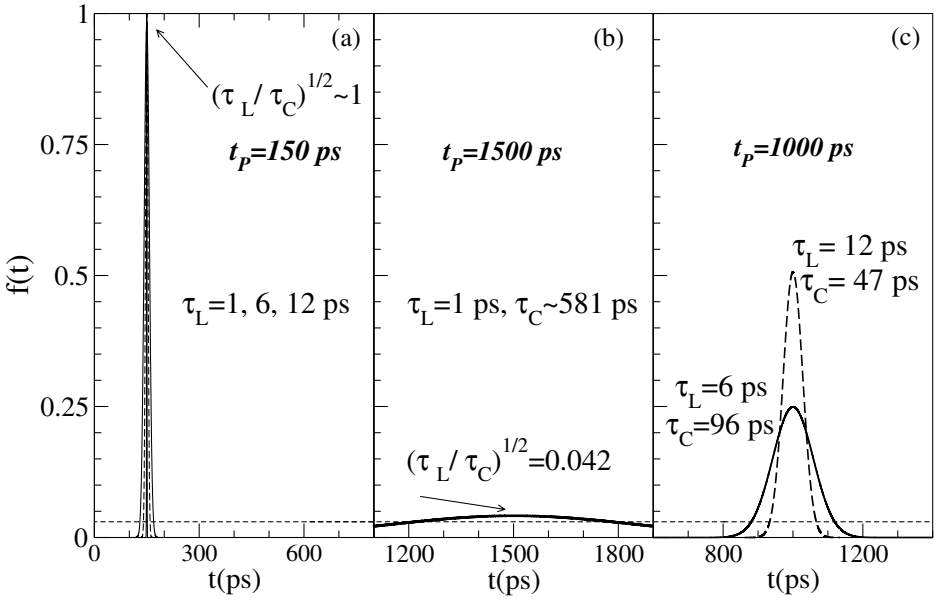

Fig. 3. Time-dependent Gaussian envelopes $f(t)$ of the linearly chirped pulses considered in this paper, all having the same chirp rate $\chi = -4.79 \times 10^{-3}$ ps^{-2} in the time domain, but different τ_L values, stretched to τ_C. At each chosen τ_L value correspond two values τ_C, as explained in the text. The maximum of the pulse, $f(t_P) = \sqrt{\tau_L/\tau_C}$, decreases when the time width τ_C increases. (a) Chirped pulses with $\tau_C \approx \tau_L = 1$ ps, 6 ps and 12 ps, centered at $t_P = 150$ ps. (b) Chirped pulse with $\tau_C = 581$ ps ($\tau_L = 1$ ps), centered at $t_P = 1500$ ps. (c) Chirped pulses with $\tau_C = 96$ ps ($\tau_L = 6$ ps) and $\tau_C = 47$ ps ($\tau_L = 12$ ps), both centered at $t_P = 1000$ ps. The horizontal broken line indicates the value from which the pulse becomes efficient in the population transfer. For the same intensity I_L of the laser, the pulses having the same initial τ_L correspond to the same energy $E_{pulse} = (I_L \tau_L/2)\sqrt{\pi/\ln 2}$, carried by the field.

5 Results for photoassociation with pulses of different durations, starting from a single scattering state $|E_0\rangle$

In the calculations presented in this section, we use as initial state a single scattering state $|E_0\rangle$, with $E_0/k_B = 54$ μK. The main characteristics of the photoassociation dynamics and of the population transferred by the pulse are analyzed with the goal of optimizing the photoassociation rate. Average over the various states $|E\rangle$ in a thermal distribution will be discussed below in Section 6.

We consider pulses generated with three initial temporal widths: $\tau_L = 1$ ps, 6 ps and 12 ps, and which are chirped with the same chirp rate in the time domain: $\chi = -4.79 \times 10^{-3}$ ps^{-2}. The characteristics of the pulses are given in Table 1. The impulsive limit is valid for all these pulses, except the pulse with $\tau_C = 581$ ps ($\tau_L = 1$ ps).

As discussed before, for fixed χ, to each given value τ_L (determining the spectral width $\delta\omega \sim 1/\tau_L$ and the total energy of the pulse $E_{pulse} \sim I_L \tau_L$) correspond two chirped pulses with very different characteristics: one has $\tau_C \approx \tau_L$, being "almost no-chirped", and the other is a "really chirped" one, having a much larger temporal width than the initial pulse. The envelopes of the 6 pulses thus built are shown in Figure 3. For each pulse we shall analyze the resulting photoassociation dynamics: the relative population yield transferred to the 0_g^- state (for a total population normalized at 1 on the grid), its radial distribution, and the modification of the density probability in the initial $a^3\Sigma_u^+(6s,6s)$ $|E_0/k_B = 54$ μK$\rangle$ state. Our aim is to analyze their efficiency for the photoassociation reaction, the main criterion being a maximum transfer of population from the initial $a^3\Sigma_u^+(6s,6s)$ $|E_0\rangle$ continuum state to bound vibrational levels of the $0_g^-(6s,6p_{3/2})$ excited state: this means that we are interested in those pulses capable to take the population located at large distances in the initial continuum and to put it in the $0_g^-(6s,6p_{3/2})$ external well, in such a way that most of this population will be present at small distances with a small delay after the end of the pulse. Maximizing the population transferred to the inner region of the excited potential ($R < 100a_0$) is a first step in a process leading to an efficient formation of cold stable molecules.

The comparison between the pulses described before can be made from two points of view: (i) one can compare "really- chirped" and "almost no-chirped" pulses, by looking at results given by the pulses with the same τ_L (the same spectral width $\hbar\delta\omega$ and the same energy E_{pulse}), and (ii) one can analyze the main differences between the results given by short pulses with a large spectral bandwidth and those given by much longer pulses with a narrower spectral width.

Several comments are to be made about what we could expect from these pulses, given the values illustrated in Table 1, and the fact that the detuning corresponding to

the $0_g^-(6s, 6p_{3/2})$ level $v_0 = 98$ excited at $t = t_P$ is $\delta_L^{at} = 2.656$ cm^{-1}.

First, we can note that the shorter pulses with $\tau_L = 1$ ps and $\tau_L = 6$ ps have the spectral widths $\hbar\delta\omega = 14.72$ cm^{-1}, much larger than $\delta_L^{at} = 2.656$ cm^{-1}, and 2.453 cm^{-1}, of the same order of magnitude as δ_L^{at}. This means that, for $\tau_L = 1$ ps, the $0_g^-(6s, 6p_{3/2})$ continuum will be massively excited. The pulses with $\tau_L = 12$ ps have the spectral bandwidth $\hbar\delta\omega = 1.227$ cm^{-1} smaller than δ_L^{at}, which avoids to noticeably populate the 0_g^- continuum (except if the intensity is too strong, see Sect. 4.3).

Second, the horizontal line in Figure 3 indicates the value above which the instantaneous coupling strength $W_L f(t)$ becomes efficient in the population transfer. The "efficient time durations" of the studied pulses are generally of the same order of magnitude as τ_C, excepting the pulse with $\tau_C = 581$ ps ($\tau_L = 1$ ps), for which the effective interval is reduced by a factor of ≈4: indeed, due to the strong decrease of W_{max} by the chirp (small ratio $\sqrt{\tau_L/\tau_C}$) only a small fraction of the pulse represented in Figure 3b can produce population transfer.

Another aspect refers to the value of the detuning $\delta_L^{at}/2 = 1.328$ cm^{-1} which is always larger than the maximum coupling W_{max} of the studied pulses (see Tab. 1). Therefore at $t = t_P$, the off-resonant Rabi coupling at very large distances R_∞ [20]:

$$\hbar\Omega(t_P, R_\infty) = \sqrt{W_{max}^2 + \left(\frac{\delta_L^{at}}{2}\right)^2} \qquad (29)$$

will be larger than the resonant coupling W_{max} at R_L (indeed, for the pulses listed in Table 1, the values of $\hbar\Omega(t_P, R_\infty)$ are between 1.3 and 1.4 cm^{-1}, the corresponding Rabi periods $T_{Rabi} = \pi/\Omega$ varying between 11 and 12.5 ps). This means that, for this small detuning, the field is strong enough to couple the two channels at very large distances, well beyond what we could expect from the estimated energy range $2\hbar|\chi|\tau_C$ resonantly swept by the pulse during the period $[-\tau_C, \tau_C]$. In fact, the off-resonance excitation at very large distances is enforced by several factors: the small detuning δ_L^{at} (corresponding to $t = t_P$), the coupling W_L, but also the much bigger overlap of the vibrational wavefunctions 0_g^- v with the initial continuum $a^3\Sigma_u^+$ $|E_0\rangle$ (see Appendix C, Fig. 12), which for $v = 160 \rightarrow 170$ ($E_v = -0.4 \rightarrow -0.2$ cm^{-1}) is about 3.7 times larger than the overlap with the state $v_0 = 98$ ($E_{v_0} = -2.6$ cm^{-1}). Lastly, the negative chirp presently studied begins resonant excitation at $t < t_P$ from the higher vibrational levels $v > 98$ of the $0_g^-(6s, 6p_{3/2})$ state. These weakly bound vibrational levels, which are excited before the maximum of the pulse at $t = t_P$, are much more sensitive at the presence of the field than the levels excited at $t > t_P$. Indeed, the time evolution of the population excited in these states shows Rabi oscillations, which are the signature of significant nonadiabatic effects, as discussed in reference [20].

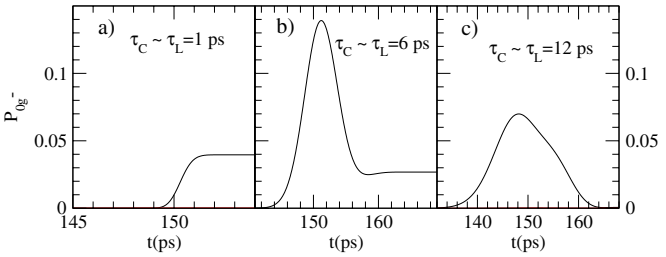

Fig. 4. Time evolution of $P_{0_g^-}(t)$, the $0_g^-(6s, 6p_{3/2})$ population (for a total population normalized at 1 on the grid) obtained by photoassociating with the "almost no-chirped" pulses having $\tau_C \approx \tau_L$, whose envelopes $f(t)$, represented in Figure 3a, are centered at $t_P = 150$ ps. In a trap of volume $V = 10^{-3}$ cm^3, containing 10^8 atoms at the temperature $T = 50$ μK, the time evolution of $\mathcal{N}_{0_g^-}(t)$, the number of molecules photoassociated per pump pulse, is related to $P_{0_g^-}(t)$ by: $\mathcal{N}_{0_g^-}(t) \sim 2000 P_{0_g^-}(t)$.

5.1 Population transferred to the $0_g^-(6s, 6p_{3/2})$ excited state

We shall discuss the time evolution of the probability for population transfer on the whole grid in the $0_g^-(6s, 6p_{3/2})$ surface:

$$P_{0_g^-}(t) = \int_0^{L_R} |\Psi_{0_g^-}(R', t)|^2 dR'. \qquad (30)$$

The relative population $P_{0_g^-}(E_0)$ transferred in the $0_g^-(6s, 6p_{3/2})$ channel after the end of the pulse ($t - t_P \gg \tau_C$) is given in Table 1. Figures 4 and 5 show the time evolution of the population $P_{0_g^-}(t)$ transferred in the $0_g^-(6s, 6p_{3/2})$ state during the photoassociation process, using the "almost no-chirped" pulses with $\tau_C \approx \tau_L = 1, 6, 12$ ps, and the "really chirped" pulses with $\tau_C = 581, 96, 47$ ps, respectively. The results shown in this section correspond to an initial population in the $a^3\Sigma_u^+(6s, 6s)$ $|E_0\rangle$ state, which is normalized to 1 on the whole grid of extension L_R. These results can be used to estimate roughly the averaged probability corresponding to the thermal distribution. Indeed, for the detuning considered, R_L is close to R_N, (see Sect. 2.3.4) so that in the range of distances governing the photoassociation process, the $R-$dependence of the initial wavefunction is the same for all energies apart from a scaling factor.Then the probability, per pump pulse, of photoassociation of a pair of atoms at the temperature $T = E_0/k_B$ is estimated to be equal to $\mathcal{P}_{0_g^-}(T) \approx P_{0_g^-}(E_0)(k_B T/(\partial E/\partial n)|_{E_0})/Z \approx 20 P_{0_g^-}(E_0)/Z$, where $k_B T$ is the width of the thermal distribution and $(\partial n/\partial E)|_{E_0}$ the density of collisional states at the energy E_0 (Z being the partition function, see Eq. (13)). The factor 20 can be estimated from equations (35) and (40) in Section 6.3 below.

We also consider the distribution of the $0_g^-(6s, 6p_{3/2})$ radialy integrated population, $P_{0_g^-}(R, t_{foc})$, as a function of the distance R, at the time $t_{foc} = t_P + T_{vib}/2 = t_P +$ 130 ps, corresponding to the focussing at the inner turning

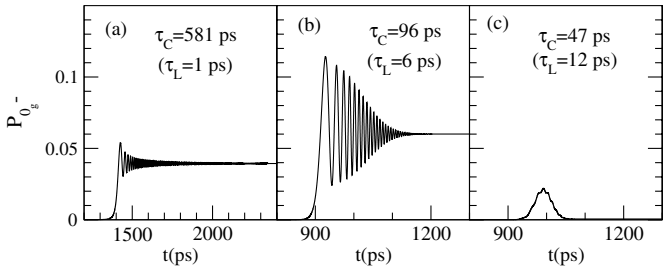

Fig. 5. Time evolution of $P_{0_g^-}(t)$, the 0_g^- population (for a total population normalized at 1 on the grid) during the photoassociation process, by using the "really chirped" pulses whose envelopes $f(t)$ are represented in Figures 3b and 3c: (a) $0_g^-(6s, 6p_{3/2})$ population for a pulse with $\tau_C = 581$ ps ($\tau_L = 1$ ps), centered at $t_P = 1500$ ps, (b) $0_g^-(6s, 6p_{3/2})$ population for a pulse with $\tau_C = 96$ ps ($\tau_L = 6$ ps), centered at $t_P = 1000$ ps, (c) $0_g^-(6s, 6p_{3/2})$ population for a pulse with $\tau_C = 47$ ps ($\tau_L = 12$ ps), centered at $t_P = 1000$ ps. In a trap of volume $V = 10^{-3}$ cm^3, containing 10^8 atoms at the temperature $T = 50$ μK, the time evolution of $\mathcal{N}_{0_g^-}(t)$, the number of molecules photoassociated per pump pulse, is related to $P_{0_g^-}(t)$ by: $\mathcal{N}_{0_g^-}(t) \sim 2000 P_{0_g^-}(t)$.

point:

$$P_{0_g^-}(R, t_{foc}) = \int_0^R |\Psi_{0_g^-}(R', t_{foc})|^2 dR'. \qquad (31)$$

At this time t_{foc} almost all the studied pulses are practically "finished", $W(t) \approx 0$, except the very large pulse with $\tau_C = 581$ ps ($\tau_L = 1$ ps), for which anyway the efficient time leading to significant transfer is over (see the dashed line in Fig. 3). For $t > t_{foc}$ the population $P_{0_g^-}$ remains constant, the two potentials 0_g^- and $a^3\Sigma_u^+$ being no longer coupled.

In Figure 6 we present $P_{0_g^-}(R, t_{foc})$, the $0_g^-(6s, 6p_{3/2})$ radialy integrated population as a function of the distance R, at the moment $t_{foc} = t_P + T_{vib}/2 = t_P + 130$ ps, for all the pulses. Results for pulses having the same τ_L are represented together, the left column showing results until $L_R = 19250 a_0$ (the limit of the spatial grid), and the right column showing the repartitions of the same populations at small distances, until $R = 140 a_0$.

At a first view the time evolutions of the 0_g^- population given by the three classes of pulses, with $\tau_L = 1$, 6, 12 ps (and with three increasing energies of the pulse E_{pulse}) are quite different, and this can be understood looking at the characteristic spectral bandwidths (see Tab. 1) and comparing them with the detuning.

As it was predicted, the two pulses with $\tau_L = 1$ ps massively populate the 0_g^- continuum (see Figs. 4a and 5a), leading at the end to the same large value of the 0_g^- population ($P_{0_g^-} = 0.04$). In this case, the spectral width $\hbar\delta\omega$ and the pulse energy E_{pulse} appear as the only parameters controlling the results, independently of the energy range $2\hbar|\chi|\tau_C$ swept during the pulse. The distributions of the 0_g^- population function of the distance R are nearly identical for both pulses (see Fig. 6a), except at short distances (Fig. 6d). It appears that due to the high value of the spectral width $\hbar\delta\omega > \delta_L^{at}$, the population is mainly transferred at very large distances $R > 1000 a_0$ (non resonantly for the "almost no-chirped" pulse with $\tau_C \approx \tau_L = 1$ ps). Only a little amount is excited at smaller distances $R < 100 a_0$, where the chirped pulse with $\tau_C = 581$ ps has a large "resonance window" (large value $\hbar|\chi|\tau_C$) and is more efficient than the short pulse of $\tau_C \approx 1$ ps, with a narrow "resonance window". It is interesting to remark that, for the pulse with $\tau_C \approx 1$ ps the population transfer is adiabatic ($\alpha_{max} > 1$) during the time window $[-\tau_C, \tau_C]$. In contrast, the adiabaticity condition cannot be satisfied for the very long pulse with $\tau_C = 581$ ps, for which α_{max} is not defined (see Tab. 1). In fact, the oscillations which can be observed in the time evolution of the 0_g^- population in Figure 5a correspond to a strong Rabi coupling at very large distances (described by Eq. (29)) and are the signature of a strong nonadiabatic behaviour in the population transfer. This non adiabatic population transfer at the large distances swept by the instantaneous crossing point results in a large population remaining in the 0_g^- surface after the end of the pulse. Similar oscillations indicating a nonadiabatic transfer can be equally observed in Figure 5b, in the evolution of the 0_g^- population during the excitation with the pulse with $\tau_C = 96$ ps ($\tau_L = 6$ ps), to whom corresponds a small value of $\alpha_{max} = 0.5$. The two other classes of pulses, with $\tau_L = 6$ and 12 ps, have narrower spectral widths, smaller than the detuning $\delta_L^{at} = 2.656$ cm^{-1}. For these cases, it appears clearly that, for the same τ_L, the "really chirped" pulse is much more efficient for the 0_g^- population transfer, both for the total transfer, as for the transfer at small distances (see Figs. 6b, 6c, 6e and 6f). The radially integrated population $P_{0_g^-}(R, t_{foc})$ is generally a overall linearly increasing function of the distance R (see Fig. 6 left column) except for the pulse with $\tau_C = 47$ ps ($\tau_L = 12$ ps), for which $P_{0_g^-}(R, t_{foc})$ reaches its limiting value at small $R \approx 140 a_0$ (Figs. 6c and 6f)), because the population transfer takes place adiabatically in a "photoassociation window" [20]. Indeed, in this case, the energy range resonantly swept by the pulse to the large distances during the period $[-\tau_C, \tau_C]$ is $\hbar|\chi|\tau_C = 1.17$ cm^{-1}, the spectral width is $\hbar\delta\omega = 1.23$ cm^{-1} (satisfying $\hbar|\chi|\tau_C + \hbar\delta\omega < \delta_L^{at}$) and the population transfer keeps an adiabatic character ($\alpha_{max} = 0.87$) both in the resonance window, and at large internuclear distances ($\Delta(R) \sim \delta_L^{at}$ for $R > 200 a_0$). On the contrary, the chirped pulse with $\tau_C = 96$ ps ($\tau_L = 6$ ps) does not produce excitation in a photoassociation window, but everywhere at large distances, because the energy range swept during the time window, satisfying $\hbar|\chi|\tau_C + \hbar\delta\omega > \delta_L^{at}$, extends above the dissociation limit ($\hbar|\chi|\tau_C \sim \hbar\delta\omega \sim 2.4$ cm$^{-1} \approx \delta_L^{at}$).

We have to remark that the very different evolutions of the 0_g^- populations during the pulses with $\tau_L = 6$ ps (see Figs. 4b and 5b), on the one hand, and with $\tau_L = 12$ ps (see Figs. 4c and 5c) on the other hand, are characteristic of two qualitatively different kinds of results: at the end of the pulse, the wavepacket created in the excited state can be spread on a wide range of distances at large R, or can be confined within a "photoassociation window". Due to

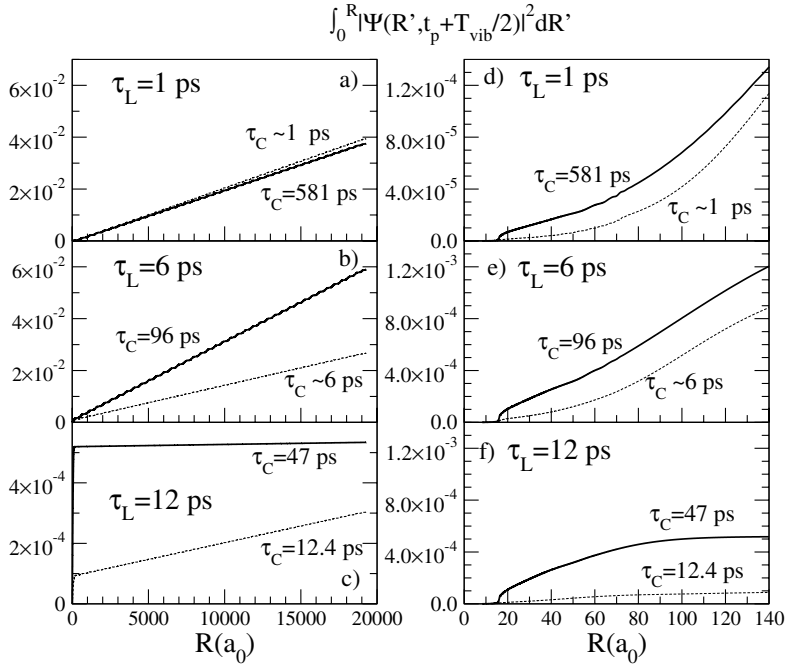

Fig. 6. Distribution of the 0_g^- radialy integrated population $P_{0_g^-}(R, t_{foc})$ at $t_{foc} = t_P + T_{vib}/2 = t_P + 130$ ps, for "really-chirped" and "almost no-chirped" pulses. Results obtained with pulses having the same τ_L (the same spectral width $\hbar\delta\omega$) are represented together: thick lines for "really-chirped" pulses ($\tau_C \gg \tau_L$), and thin lines for "almost no-chirped" pulses ($\tau_C \approx \tau_L$). Left column: distribution of the 0_g^- population until $L_R = 19250a_0$. Right column: population until $R = 140a_0$. "Really-chirped" pulses give a much larger population transfer in the 0_g^- state, as the spanned energy range $2\hbar|\chi|\tau_C$ is much larger; they give also much more population at small distances (the results show the population in the 0_g^- channel relative to a total population normalized at 1 on the grid. Multiplying the vertical axis by a factor equal to 2000 gives the distribution of the 0_g^- radialy integrated number of molecules $\mathcal{N}_{0_g^-}(R, t_{foc})$ at t_{foc}, in a trap of volume $V = 10^{-3}$ cm^3, containing 10^8 atoms at the temperature $T = 50$ μK).

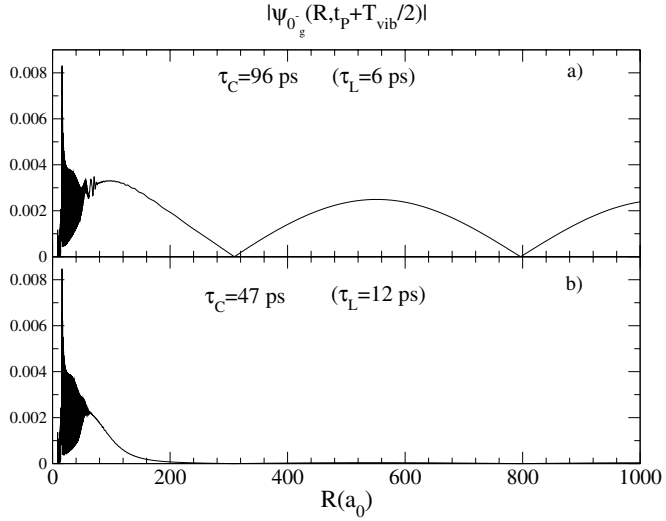

Fig. 7. Excited wavepackets focalized at $t_{foc} = t_P + T_{vib}(v_0)/2$ at the inner turning point of the outer well of the 0_g^- potential. Comparison of two typical final states: (a) transfer at large distances, and (b) excitation in a "photoassociation window".

the large amplitude of the initial continuum wavefunction at large R, it is expected that more population should be transferred in the first case.

This is illustrated in Figure 7 showing the 0_g^- wavepackets at $t_{foc} = t_P + T_{vib}/2 = t_P + 130$ ps, (a) for the chirped pulse with $\tau_C = 96$ ps ($\tau_L = 6$ ps), giving population transfer on the whole spatial grid, and (b) for the chirped pulse with $\tau_C = 47$ ps ($\tau_L = 12$ ps), producing transfer in a "photoassociation window". Due to the choice of the χ value, at $t_{foc} = t_P + T_{vib}(v_0)/2$ both wavepackets, in the R-range corresponding to the outer well of the 0_g^- potential, are focussed at the inner turning point of the vibrational eigenstate v_0 excited at $t = t_P$.

We are especially interested in pulses producing the maximum transfer of 0_g^- population to the small and intermediate distances (see Fig. 6 for this analysis). From this point of view, the pulses with $\tau_L = 6$ ps ($\tau_C = 96$ ps and $\tau_C = 6.012$ ps) and the pulse with $\tau_C = 47$ ps ($\tau_L = 12$ ps) are giving the bigger population at small R. Their results can be seen and compared in Figures 6e and 6f. At $t_{foc} = t_P + T_{vib}/2$, both pulses with $\tau_C = 6.012$ ps ($\tau_L =$ 6 ps) and with $\tau_C = 47$ ps ($\tau_L = 12$ ps) give $P_{0_g^-}(100a_0, t_{foc}) \approx 4 \times 10^{-4}$, but the pulse with $\tau_C = 47$ ps, which produces a "photoassociation window", is more favorable to transfer population at smaller R-values $R < 100a_0$. Nevertheless, it is the pulse with $\tau_C = 96$ ps ($\tau_L = 6$ ps) which seems to be the most efficient for the 0_g^- population transfer, at large distances, but also to the inner region ($P_{0_g^-}(100a_0, t_{foc}) \approx 8 \times 10^{-4}$), because even after the end

of the pulse, the population will be accelerated inside from the large distances.

Let's remark that, as discussed in reference [26], the negative chirp has a noticeable contribution in the acceleration of the wavepacket created in the excited state 0_g^- towards short internuclear distances. Indeed, $\omega(t)$ decreasing with time, the instantaneous crossing point moves to smaller distances, following the motion of the wavepacket which is accelerated inside the potential well. This is favorable to our goal of maximizing 0_g^- population at small distances. On the other hand, this means that an interpretation of the transfer process within the impulsive approximation could easily be invalidated. For example, in our case, the population in the initial continuum state integrated until $R = 100a_0$ is:

$$\int_0^{R=100} \left|\Psi_{\Sigma,T=54\mu K}(R')\right|^2 dR' = 3 \times 10^{-4} \qquad (32)$$

and, if the impulsive approximation was valid until $t = t_{foc}$, this integral (32) gives an upper limit for the integral $\int_0^{R=100} |\Psi_{0_g^-}(R', t_{foc})|^2 dR'$. But we have shown that, in the cases of some of the pulses discussed before, (with $\tau_C \approx 6$ ps, $\tau_C = 96$ ps and $\tau_C = 47$ ps), $P_{0_g^-}$ ($100a_0$, t_{foc}) reaches indeed bigger values, proving the acceleration towards shorter internuclear distances for times $t < t_{foc}$.

5.2 Population in the last vibrational levels of the ground state

In the non perturbative regime there is a redistribution of population in the ground surface $a^3\Sigma_u^+(6s, 6s)$, arising as well in the bound spectrum, as in the dissociation continuum. There appears a "hole" in the initial wavefunction around R_L, a large part of this population being transferred in bound vibrational levels of 0_g^- and $a^3\Sigma_u^+$.

Due to the coupling at large distances between the two electronic states, the last vibrational levels of the $a^3\Sigma_u^+(6s, 6s)$ state are noticeably populated during the photoassociation process. Figures 8 and 9 show the evolution of the population in these last levels ($v'' = 53$ is the last vibrational level [20]). If one compares pulses with the same τ_L, the final transferred population is roughly of the same order, but for $\tau_L = 1$ or 12 ps it is bigger for "almost no-chirped" pulses, probably because the maximum coupling W_{max} is more intense for shorter pulses. The pulses with $\tau_L = 6$ ps ($\tau_C = 6.012$ ps and 96 ps) give almost the same population of $v'' = 52$, 53. In Figure 9b we show the Rabi oscillations in opposite phase between the 0_g^- population $P_{0_g^-}$ (which is distributed on the whole spatial grid of $L_R = 19250a_0$) and the population of the last vibrational state of the $a^3\Sigma_u^+(6s, 6s)$, with $v'' = 53$, whose wavefunction extends at very large distances (the last oscillation is between 150 and $1200a_0$, see Fig. 2a). This result is symptomatic for the efficient exchange of population between the two channels at very large distances, already emphasized, and due to the small detuning and large overlap integral (see Appendix C, Fig. 12). Around $t_p = 1000$ ps, the period of the observed Rabi oscillations is about 12.4 ps, in agreement with the result given by the formula (29). The oscillations which can be observed in Figures 9a and 9b are characteristic for nonadiabatic effects in the transfer of populations.

One has to emphasize that, in the cases of adiabatic transfer in a limited spatial window (for example, here with the pulse $\tau_C = 47$ ps, and in reference [20] with a pulse having $\tau_C = 34.8$ ps), the populations, at the end of the pulse, in the last bound states $v'' = 52$, 53 of the ground potential, are of the same order as the populations $P_{0_g^-}$ of the 0_g^- levels resonantly excited by the pulse in the so-called "photoassociation window". For example, for the pulse with $\tau_C = 47$ ps, $P_{0_g^-}(E_0) = 5.34 \times 10^{-4}$ (see Tab. 1), and the population $P_{^3\Sigma_u^+}(v'' = 52) + P_{^3\Sigma_u^+}(v'' = 53) \approx 2.25 \times 10^{-4}$ (see Fig. 9c). But we should note that for $v'' = 52$, 53 the vibrational wavefunctions, extending up to hundreds of a_0, have a good overlap with wavefunctions in the excited state corresponding to levels close to the dissociation limit and transiently populated during the pulse. In contrast, the 0_g^- levels populated within the "photoassociation window" have a vibrational motion restricted to much smaller distances, since their outer turning points are between $R_{min} = 84a_0$ and $R_{max} = 117a_0$: they remain populated after the pulse [20].

5.3 Evolution of the 0_g^- wavepacket after the pulse

We shall briefly describe the wavepackets evolution in the 0_g^- surface after the pulse, in the two typical cases discussed before: excitation in a limited spatial "photoassociation window" and excitation at all distances, with massive transfer of population at large distances. Obviously, these two types of wavepackets created by the photoassociating pulse are extremely different, and their dynamics is significant in view of some anticipation of the results that could be brought by a second pulse. This second pulse can be even identical with the first one, but time-delayed (in the analysis of the repetition rate of the laser) or a different pulse, if the goal is the stabilization of the system by stimulated emission to low vibrational levels of the ground state. These subjects will be treated in a future article.

5.3.1 Excitation in "a window": vibrational dynamics

Figure 10 shows the evolution of the 0_g^- wavepacket adiabatically excited ($\alpha_{max} = 0.87$) in a limited spatial window, with a chirped pulse of time width $\tau_C = 47$ ps ($\tau_L = 12$ ps). In fact, during the pulse, a large amount of population is transferred to levels close to the $Cs_2(6s + 6p_{3/2})$ dissociation limit (see the wavepacket at $t = t_P$, in Fig. 10a), but, due to the adiabaticity of the population transfer outside the "photoassociation window", this population goes back to the ground state and only a small range of distances ($R < 200a_0$) remains populated. Then, after the pulse, one can observe a typical vibrational dynamics, as it can be seen in the figure for some

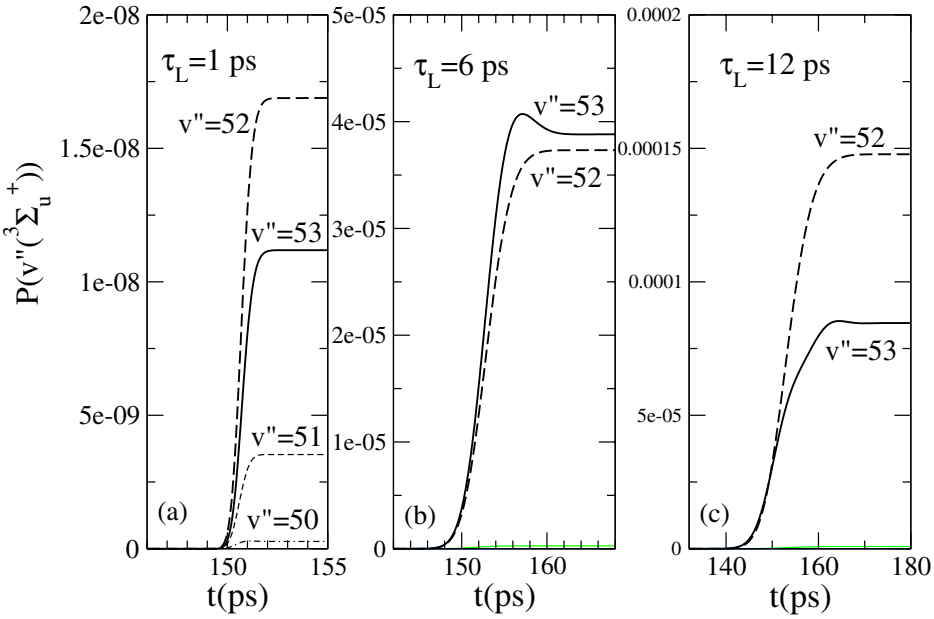

Fig. 8. Populations in the last vibrational levels v'' ($a^3\Sigma_u^+(6s,6s)$) of the ground state, for "almost no-chirped" pulses ($\tau_C \approx \tau_L$). (The total population is normalized at 1 on the grid.) Multiplying the vertical axis by a factor equal to 2000 gives the number of molecules in the last vibrational levels v'' of the ground state for a trap of volume $V = 10^{-3}$ cm^3, containing 10^8 atoms at the temperature $T = 50$ μK.

selected times: at $t = t_P + T_{vib}(v_0)/2$ the packet is focalized at the inner turning point of v_0, at $t = t_P + T_{vib}(v_0)$ the packet comes back at the external turning point of v_0 ($R_L = 93.7a_0$), at $t = t_P + 2T_{vib}(v_0) \approx t_P + 500$ ps, one can distinguish two parts: one, with a maximum around $R_L = 93.7a_0$, is composed by levels with vibrational periods close to $T_{vib}(v_0)$; the other has a maximum around $R = 130a_0$: indeed, the vibrational levels of the 0_g^- potential having the external turning point around this distance vibrate with $T_{vib} \approx 500$ ps.

5.3.2 Excitation at large distances: acceleration to the inner region

For pulses having sufficiently large bandwidths ($\delta\omega > \delta_L^{at}$), the population transferred at large distances during the pulse remains on the excited surface 0_g^- after the end of the pulse. Just after the end of the pulse, the radial distribution $|\Psi_{0_g^-}(R,t)|^2$ of the probability density reproduces that of the initial collisional state on the $^3\Sigma_u^+$ surface at sufficiently large distances $R > 500a_0$. After that, the wavepacket evolves in the $-C_3/R^3$ potential and it is accelerated toward the inner region. Figure 11 describes the evolution of the wavepacket created by the pulse with $\tau_C = 96$ ps ($\tau_L = 6$ ps), at different moments $t_P + \Delta t$, with $\Delta t = 0.1$, 4, 9, and 14 ns. As it can be seen in Figure 11a, for $R \geq 1500a_0$, there is no noticeable modification of the probability density $|\Psi_{0_g^-}(R,t)|^2$, even for the largest value of Δt. As Δt increases, the nodes occuring at $R \geq 500a_0$ ($R_1 \approx 800a_0$ and $R_2 \approx 1270a_0$, for example) begin to be shifted toward small R values. In the range $R \leq 500a_0$, vibrational motion can be observed winning progressively distances indicated as R_{vib} on the figures, corresponding to the outer turning point of the bound level with the vibrational period $T_{vib} \approx \Delta t$. For example, for $\Delta t = 14$ ns (see Fig. 11a.4), one has $R_{vib} = 490a_0$ which corresponds to the outer turning point of the vibrational level $v = 162$ with vibrational period $T_{vib} \approx 13.7$ ns. (The largest time $\tau_{max} = 2.9$ μs relevant for the presently used grid with $L_R = 19250a_0$ correspond to vibrational motion at distances $R \approx 4000a_0$.)

The acceleration of the 0_g^- wavepacket can be estimated introducing the radial flux [42]:

$$J_{0_g^-}(R,t) = -\frac{i\hbar}{\mu}\mathrm{Im}\left[\Psi^*_{0_g^-}(R,t)\frac{\partial}{\partial R}\Psi_{0_g^-}(R,t)\right], \qquad (33)$$

with $\mu = 121136$ a.u. the reduced mass of Cs_2. Writing the wavepacket as $\Psi_{0_g^-}(R,t) = |\Psi_{0_g^-}(R,t)|e^{i\phi_{0_g^-}(R,t)}$, one has $p_{0_g^-}(R,t)/\hbar = (\mu/\hbar)J_{0_g^-}(R,t)/|\Psi_{0_g^-}(R,t)|^2 = \partial\phi_{0_g^-}(R,t)/\partial R$. Figure 11b reports the R-variation of the momentum $p_{0_g^-}/\hbar$ at the times $t_p + \Delta t$; the rapid increase at intermediate R values $200a_0 \leq R \leq 700a_0$, for 0.1 ns $< \Delta t <$ 5 ns is clearly illustrated. This increase in the momentum transfer during the pulse is a signature of the "kick" given by the laser light to the molecule. For "really chirped" pulses the photoassociation probability is relatively important, and the population transferred at intermediate distance is accelerated to the inner region a short time after the end of the pulse, increasing significantly the population at short distances. Optimization of the pulse parameters in order to create wavepackets at intermediate distances, with a strong momentum in the direction of the inner region, will be considered in the future.

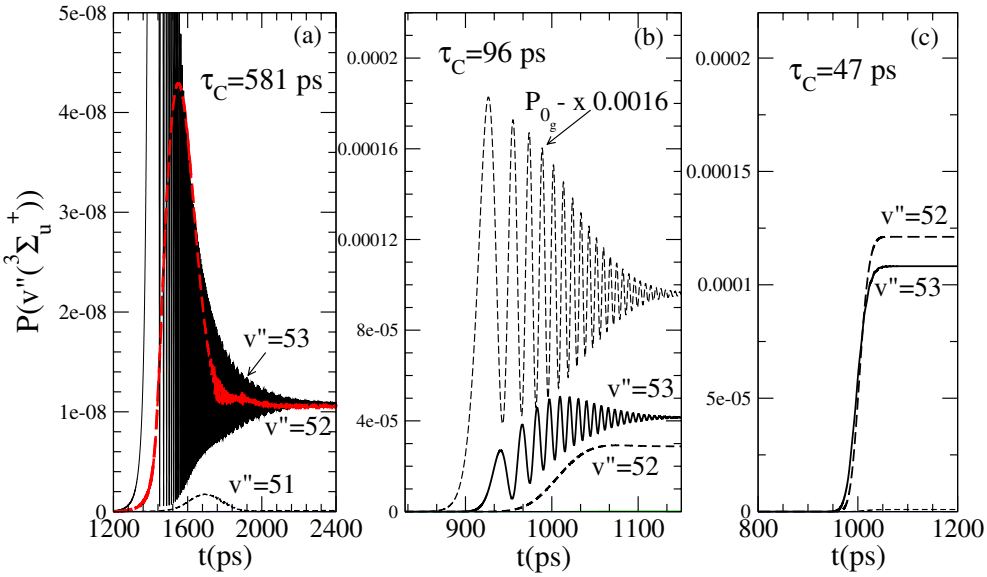

Fig. 9. Populations in the last vibrational levels v'' ($a^3\Sigma_u^+(6s,6s)$) of the ground state for chirped pulses with $\tau_C = 581$ ps, 96 ps, and 47 ps. (The total population is normalized at 1 on the grid.) Multiplying the vertical axis by a factor equal to 2000 gives the number of molecules in the last vibrational levels v'' of the ground state for a trap of volume $V = 10^{-3}$ cm^3, containing 10^8 atoms at temperature $T = 50$ μK.

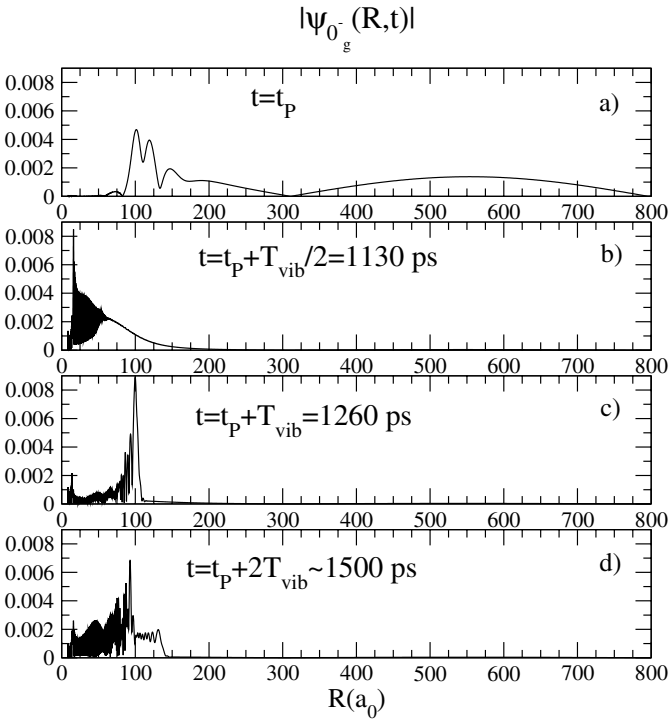

Fig. 10. 0_g^- wavepackets evolution after the pulse with $\tau_C = 47$ ps ($\tau_L = 12$ ps).

6 Photoassociation probability from a thermal average over the incident kinetic energies

Supposing thermal equilibrium at the temperature T, the initial density matrix can be expressed in terms of energy-normalized collisional eigenstates of energies E in the ground state $a^3\Sigma_u^+$, as in the formula (12). Then the total probability per pump pulse that a given pair of atoms to be photoassociated into the excited state 0_g^- at the temperature T, is:

$$\mathcal{P}_{0_g^-}(T) = \frac{1}{Z}\int_0^\infty dE e^{-\beta E}\bar{P}_{0_g^-}(E), \qquad (34)$$

where $\bar{P}_{0_g^-}(E)$ accounts for the density of probability (probability per unit energy range) that an energy normalized continuum state of energy E belonging to the ground state $a^3\Sigma_u^+$ to be photoassociated at the end of the pulse in the excited state 0_g^-. $\bar{P}_{0_g^-}(E)$ has dimension of $1/E$, being obtained with the formula (50) from the dimensionless photoassociation probability $P_{0_g^-}(E)$ in the 0_g^- state:

$$\bar{P}_{0_g^-}(E) = \left\{\frac{\partial E}{\partial n}\right\}^{-1} P_{0_g^-}(E). \qquad (35)$$

We shall discuss in the following the evaluation of the integral (34).

6.1 Analytical thermal average using the scaling law in the vicinity of E → 0

In reference [20] and in the most part of this paper we present results of photoassociation calculations considering only the s-wave and taking as the initial state in the $a^3\Sigma_u^+(6s,6s)$ ground potential a single continuum state of the thermal energy distribution, with the energy E_0. In our calculation $E_0 = 1.7211 \times 10^{-10}$ a.u. $= 3.778 \times 10^{-5}$ cm^{-1}, being, in our method, the energy of a continuum state belonging to the discretized continuum

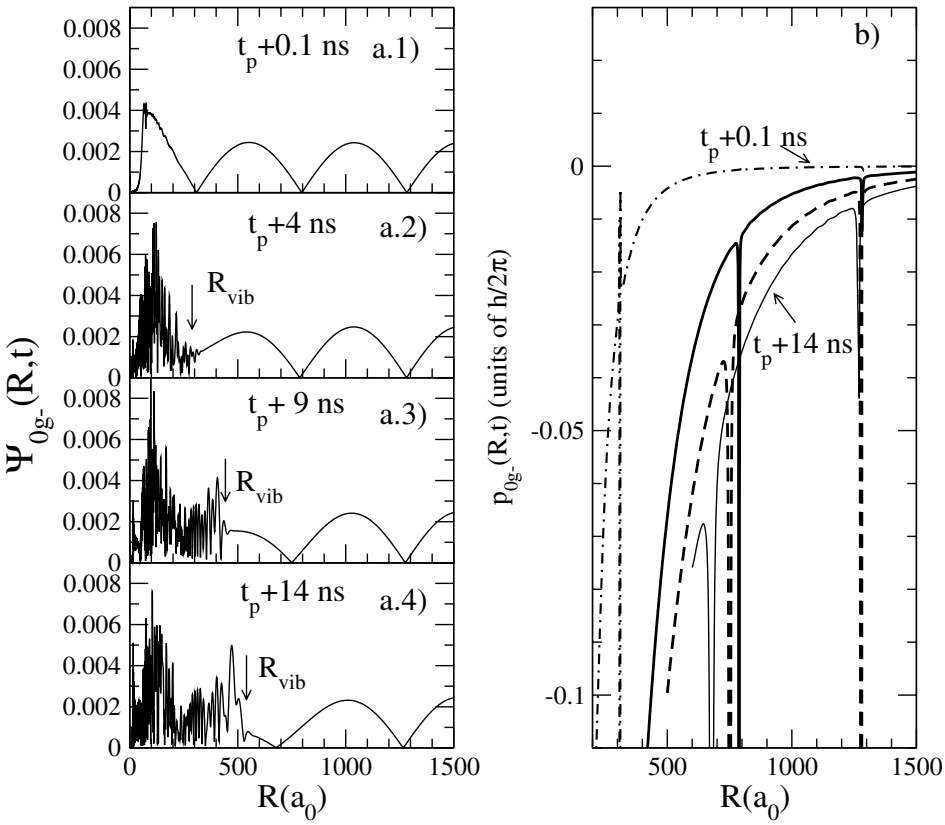

Fig. 11. (a.1–a.4) 0_g^- wavepackets evolution after the pulse with $\tau_C = 96$ ps ($\tau_L = 6$ ps), at different moments after the end of the pulse (whose maximum is at $t_P = 1000$ ps): $t = t_P + 0.1$ ns, $t_P + 4$ ns, $t_P + 9$ ns, $t_P + 14$ ns. (b) The R-variation of the momentum $p_{0_g^-}(R,t)/\hbar$ at the same times: $t_P + 0.1$ ns (dot-dashed line), $t_P + 4$ ns (thick continuum line), $t_P + 9$ ns (dashed line), $t_P + 14$ ns (thin continuum line), showing the acceleration of the wavepacket to the inner region. The singularities in the momentum behaviour are due to the definition modulo π of the phase, and correspond to the nodes of the wavepacket according to the Milne's equation [41] relating the derivative of the phase of the wavepacket and its amplitude.

which is calculated numerically with the Sine Mapped Grid method in a box of radius $L_R = 19250a_0$. Then, with this choice of the initial continuum state, the temperature in the thermal ensemble of atoms is arbitrarily defined by $k_BT = E_0$, as being $T = 54$ μK. At this temperature, the initial Boltzmann distribution (see formula (12)) is narrow ($e^{-3} = 0.05$), and a first approximation is to represent it by its mean energy E_0, which is justified by the fact that the spectral widths $\hbar\delta\omega$ of the pulses considered in photoassociation (see Tab. 1) are much larger than k_BT. Then, the integral (34) can be evaluated from $\bar{P}_{0_g^-}(E_0)$, by using a threshold scaling law to estimate the probabilities $\bar{P}_{0_g^-}(E)$ for $E \neq E_0$ [16].

We shall discuss the conditions making valid the use of the scaling law for estimations of the photoassociation rates. We emphasize that such a discussion makes sense only for the photoassociation with a cw-laser or with a pulse leading to the formation of a spatially localized wavepacket on the excited surface [16,20], giving what we have called a "photoassociation window". In such a case, the main contribution to the photoassociation process towards high excited vibrational levels is provided by the very localized range of the internuclear distances $[R_{min}, R_{max}]$, around $R \sim R_L$, swept by the instantaneous crossing point $R_c(t)$ during the time window $[-\tau_c, \tau_c]$ [20]. The photoassociation yield is determined by the overlap between the initial stationary continuum $|^3\Sigma_u^+, E\rangle$ in the ground state and the excited wavefunctions $|0_g^-, v\rangle$ (see Appendix C, Fig. 12).

A scaling law for the behaviour of the continuum wavefunctions can be obtained from their asymptotic forms. For a very small detuning δ_L^{at}, the crossing point R_L of the dressed potentials is at a distance large enough making that, even at a low continuum energy E, the potential in R_L can be considered as negligible: $E > C_6/R_L^6$. Then, for a s-wave, the continuum wavefunction can be described by its asymptotic behaviour [46]:

$$|\Psi_{g,E}(R)| \approx \sqrt{\frac{2\mu}{\pi\hbar^2}} \frac{\sin[k(R-L)]}{\sqrt{k}} \tag{36}$$

L is the scattering length of the ground surface. This means that, for sufficiently low collision energies:

$$E \ll \frac{1}{2\mu} \left| \frac{\pi\hbar}{R_L - L} \right|^2 = k_B T_{an} \tag{37}$$

one obtains the following probability density in R_L:

$$|\Psi_{g,E}(R_L)|^2 \approx \frac{2\mu}{\pi\hbar^2}k(R_L - L)^2 \sim \sqrt{E} \tag{38}$$

as $E = (\hbar k)^2/2\mu$. Then, for pulses producing a spatially localized wavepacket on the excited surface, and for sufficiently small energies, one can assume the following law for the probabilities $\bar{P}_{0_g^-}(E) \sim |\Psi_{g,E}(R_L)|^2$:

$$\bar{P}_{0_g^-}(E) = \bar{P}_{0_g^-}(E_0)\sqrt{E/E_0}. \tag{39}$$

Using the relation (39), the integral (34) can be evaluated as being:

$$\mathcal{P}^{an}_{0_g^-}(T) = \frac{1}{Z}\bar{P}_{0_g^-}(E_0)\frac{\sqrt{\pi}}{2\sqrt{E_0}}(k_B T)^{3/2} \tag{40}$$

$\mathcal{P}^{an}_{0_g^-}(T)$ represents the probability that a pair of atoms, belonging to a gas in a volume V and at the temperature T, and described only by s-waves, to be photoassociated in the $0_g^-(6s + 6p_{3/2})$ state.

For a typical number which can be obtained for this quantity, we shall take as example the pulse studied in great detail in reference [20], whose characteristics are given in Table 1, and having the duration $\tau_C = 34.8$ ps ($\tau_L = 15$ ps). The induced dynamics (which is very similar to that resulting from the "really chirped" pulse with $\tau_C = 46.6$ ps and $\tau_L = 12$ ps) results in an adiabatic population transfer in a spatial range with $R_{min} = 85a_0$, $R_{max} = 110a_0$, with $\alpha_{max} = 0.95$, and populating about 15 vibrational levels in the vicinity of $v_0 = 98$ level in the external well of the $0_g^-(6s+6p_{3/2})$ potential. It corresponds to the photoassociation probability $P_{0_g^-}(E_0) = 3.245 \times 10^{-4}$. Then, taking into account the density of states $dn/dE|_{E_0} = 1.1415 \times 10^{11}$ a.u. at $E_0/k_B = 54.35$ μK, for a gas of cesium atoms at $T = 54$ μK we have used the formula (40) to obtain:

$$Z\mathcal{P}^{an}_{0_g^-}(T = 54\ \mu\text{K}, \tau_C = 34.8\ \text{ps}) = 0.00560 \tag{41}$$

with τ_C characterizing the pulse used for photoassociation.

6.2 Average implicitly accounting for real threshold effects

As discussed in a previous section, in the conditions of temperature and detuning discussed in the present paper, the asymptotic behaviour of the continuum wavefunction having the energy $E_0 = k_B T$, $T = 54$ μK, is not reached at $R = R_L = 94a_0$. Indeed, the potential energy strongly determines the structure of the initial wavefunction for $R \leq R_N = 82.3a_0$, R_N being the position of the last common node. This observation is in agreement with the discussion of reference [46], showing that the asymptotic behaviour in a $-C_6/R^6$ potential is reached for $R \gg R_B = (\mu C_6/10\hbar^2)^{1/4}$, giving $R_B = 95a_0$ for the $^3\Sigma_u^+(6s, 6s)$ potential.

Then, in the present studied example of cold atoms photoassociation, the detuning $\delta_L^{at} = 2.656$ cm^{-1} is too large ($R_L \approx R_N$), and the temperature $T = 54$ μK not sufficiently small compared to $T_{an} = 69.2$ μK (see the relation (37)), to allow the evaluation of the photoassociation rate from an analytical thermal average. The scaling law in $\sqrt{E}$ being not valid, it is necessary to explicitly study the energy variation of $\bar{P}_{0_g^-}(E)$, by considering different initial collisional states of energy E in the $^3\Sigma_u^+$ potential, and having a node at L_R. In this case, the real threshold effects are completely and correctly accounted for implicitly by performing numerical integration in equation (34). For example, for the pulse with $\tau_C = 34.8$ ps ($\tau_L = 15$ ps) studied in reference [20], we have performed 21 time-propagation calculations for collisional energies in the range 36.6 nK $< E/k_B <$ 633 μK. Let us emphasize that this detailed analysis of the threshold effects has become possible owing to the Mapped Sine Grid method [30] for which a large box of dimension L_R can be considered. The energy-dependence of $\bar{P}_{0_g^-}(E)$ will be analyzed in a further publication [43]. It differs strongly from the $\sqrt{E}$ scalling law. $\bar{P}_{0_g^-}(E)$ increases very rapidly at threshold exhibiting a very sharp asymmetrical resonance like structure with a maximum at $E/k_B \approx 7.9$ μK (smaller than the temperature studied presently) with a FWHM $\Delta E/k_B \approx 4.7$ μK. For the temperature $T = 54$ μK, numerical integration in equation (34) leads to

$$Z\mathcal{P}_{0_g^-}(T = 54\ \mu\text{K}, \tau_C = 34.8\ \text{ps}) = 0.00685. \tag{42}$$

The rather good agreement between the analytic average (41) calculated with the scaling law, and the average (42) containing the threshold effects is completely fortuitous.

The two pulses described by the same parameters δ_L^{at}, W_L and χ, and differing only by their durations $\tau_C = 34.8$ ps ($\tau_L = 15$ ps) and $\tau_C = 46.6$ ps ($\tau_L = 12$ ps) are associated with rather similar "photoassociation windows" characterized by the values ($\alpha_{max} = 0.95$, $\hbar|\chi|\tau_C = 0.87$ cm^{-1}) and ($\alpha_{max} = 0.87$, $\hbar|\chi|\tau_C = 1.17$ cm^{-1}). For the same initial collisional state $E_0/k_B = 54.35$ μK, the corresponding photoassociation probabilities are $P_{0_g^-}(E_0) = 3.245 \times 10^{-4}$ and 5.340×10^{-4}. The photoassociation probability is larger for the longer pulse with $\tau_C = 46.6$ ps ($\tau_L = 12$ ps), which creates a slightly larger photoassociation window ($R_{min} = 84a_0$, $R_{max} = 117a_0$), compared to ($R_{min} = 85a_0$, $R_{max} = 110a_0$) for the pulse with $\tau_C = 34.8$ ps ($\tau_L = 15$ ps). This increase of $P_{0_g^-}(E_0)$ has to be related to the increase of the probability density within the photoassociation window in the initial collisional state ($\int_{R_{min}}^{R_{max}} |\Psi_{\Sigma,E_0}(R')|^2 dR' = 0.00044$ and 0.00076, see also Ref. [20], Fig. 3), which is a signature of the nearly total population transfer in this range of R.

For the pulse with $\tau_C = 34.8$ ps ($\tau_L = 15$ ps) we have shown that the energy dependence of $\bar{P}_{0_g^-}(E)$ is proportional to that of the square of the overlap integral $|\langle 0_g^- \ v_0 = 98|^3\Sigma_u^+ \ E\rangle|^2$ [43]. Taking into account the

very similar dynamics induced by the two pulses with $\tau_C = 34.8$ ps ($\tau_L = 15$ ps) and $\tau_C = 46.6$ ps ($\tau_L = 12$ ps), it is reasonable to assume that the energy variation of $\bar{P}_{0_g^-}(E)$ is the same for both pulses. Therefore, for the same temperature, both pulses correspond to the same value of the ratio $\mathcal{P}_{0_g^-}(T)/\bar{P}_{0_g^-}(E_0)$, and the total probability per pump pulse $\tau_C = 46.6$ ps ($\tau_L = 12$ ps) that a given pair of atoms to be photoassociated into the 0_g^- state at a temperature $T = 54$ μK can be estimated to:

$$Z\mathcal{P}_{0_g^-}(T = 54\ \mu\text{K}, \tau_C = 46.6\ \text{ps}) = 0.0113. \quad (43)$$

6.3 Total number of molecules photoassociated per pump pulse

For a number of N atoms in a volume V, the number of pairs of atoms is $N(N-1)/2 \approx N^2/2$. Taking into account the spin degeneracy of the Cs(6^2S) atomic state, $d_A = 2$, and of the initial electronic state $d_{^3\Sigma_u^+} = 3$, the total number of molecules photoassociated in the excited state 0_g^- per pump pulse is:

$$\mathcal{N} = \frac{N^2}{2}\mathcal{P}_{0_g^-}(T)\frac{d_{^3\Sigma_u^+}}{d_A^2}. \quad (44)$$

For a trap of volume $V = 10^{-3}$ cm^3, at the temperature $T = 54$ μK and with a density of atoms $N_A = N/V = 10^{11}$ cm^{-3}, the partition function is $Q(T) = 59.86 \times 10^{-10} a_0^{-3} = 40.4 \times 10^{15}$ cm^{-3}. Then the number of molecules photoassociated per pump pulse is:

$$\mathcal{N}_{(\tau_C=34.8\ \text{ps})} = 0.69, \quad \mathcal{N}_{(\tau_C=46.6\ \text{ps})} = 1.40. \quad (45)$$

Using equations (35) and (40), for a trap of volume $V = 10^{-3}$ cm^3, containing 10^8 atoms at the temperature $T = 50$ μK, it is possible to relate the number of molecules photoassociated per pump pulse $\mathcal{N}$ to the probability of photoassociation in the 0_g^- surface $P_{0_g^-}(E_0)$, corresponding to a total population normalized to 1 on the grid, by: $\mathcal{N} \sim 2000 P_{0_g^-}(E_0)$.

For a repetition rate equal to 10^8 Hz and supposing that each pulse acts on the same initial state, this gives 6.9×10^7 molecules per second for the pulse with $\tau_C = 34.8$ ps ($\tau_L = 15$ ps) and 1.4×10^8 molecules per second for the pulse with $\tau_C = 46.6$ ps ($\tau_L = 12$ ps).

The analysis of the energy-dependence of the photoassociation probability $\bar{P}_{0_g^-}(E)$ for pulses leading to significant population transfer at large internuclear distances is in progress.

7 Discussion: possible ways for optimization

From the previous analysis, we may extract some directions on possible ways of optimizing the pulse. In the situation where the population transfer occurs mainly within the photoassociation window, for sufficiently large coupling W_{max}, the total adiabatic population transfer implies that the whole population for pair of atoms with relative distance lying in the $[R_{min}, R_{max}]$ range, $P_{init} = \int_{R_{min}}^{R_{max}} |\Psi_{g,E_0}(R', t = 0)|^2 dR'$, is transferred to bound levels of the excited state and to the last bound levels of the ground state. The photoassociation yield can be optimized by designing the chirped pulse in order to maximize P_{init}. This can be achieved by increasing the photoassociation window with τ_C values as large as possible, under the condition $\hbar(\delta\omega + |\chi|\tau_C) \leq \delta_L^{at}$ so that only bound levels are populated. This yields an optimal value for τ_L which is $\tau_{opt} \sim 8\hbar \ln 2/\delta_L^{at}$. Since the condition (28) is fixing an upper value for τ_L to make focalization possible, we end with an upper limit for the detuning, and optimization can be achieved making use of the scaling laws governing the spectra of long range molecules. This will be further explored in future work, but for the detuning $\delta_L^{at} = 2.652$ cm^{-1} considered here, it is clear that the optimal pulse would be $\tau_L \sim 10$ ps, corresponding to $P_{init} = 1.27 \times 10^{-3}$, i.e. to a photoassociation rate increased by a factor 2.4 compared to the pulse with $\tau_C = 47$ ps ($\tau_L = 12$ ps), considered in the present work.

We have also obtained an increase of the population by a factor of 4.3 when considering the pulse $\tau_C = 34.8$ ps ($\tau_L = 15$ ps), and increasing the coupling by a factor of 16, corresponding to a peak intensity $I_L = 3.36$ MW cm^{-2} for the transform limited pulse.

Finally, we should remind that the present choice for the detuning corresponds to a minimum in the cw photoassociation spectrum [6]. An increase by a factor of 5 on the probability reported in the last column of Table 1 was obtained, by reducing the detuning to 0.0695 cm^{-1} (therefore moving the value of R_L to $150a_0$) in case of a pulse with $\tau_C = 110$ ps ($\tau_L = 58$ ps) (corresponding to the present result for $\tau_C = 47$ ps, $\tau_L = 12$ ps). The number of molecules formed in the conditions of Section 6.3 would reach 7×10^8 molecules per second, so that in less than 70 ms all the pairs of atoms are transformed to molecules.

8 Conclusion

We have investigated the possibilities offered by chirped laser pulses to optimize the yield of the photoassociation process. Following a previous paper [20], time-dependent calculations have been presented for the particular example of the reaction $(\text{Cs}(6s) + \text{Cs}(6s))^3\Sigma_u^+ \rightarrow \text{Cs}_2\, 0_g^-\ (6s + 6p_{3/2})$ involving ground state cesium atoms at a temperature $T \sim 54$ μK. These cold collisions occur in presence of laser pulses of different spectral widths $\delta\omega$ and with the same linear chirp rate in the time domain $\chi = -4.79 \times 10^{-3}$ ps^{-2}. The central frequency is red-detuned by $\delta_L \sim 2.65$ cm^{-1} relative to the D_2 atomic line and excites at resonance the $v_0 = 98$ vibrational level in the outer well of the 0_g^- level potential. The new aspects in the present work are:

– (i) the calculations take into account the mixed state character of the initial collision state, described by a statistical mixture of stationary collision eigenstates

representing thermal equilibrium at $T \sim 54$ μK. This choice reproduces correctly the spatial delocalization of the initial state, with large de Broglie wavelength $\lambda_{\rm DB} \sim 975 a_0$. In the range of detunings considered here, experiments with a cw laser have demonstrated minima in the photoassociation rate corresponding to the nodes in the scattering wavefunctions: such nodes, common to the various eigenstates, are correctly reproduced in the present treatment. The continuum wavefunctions are represented as eigenstates in a large box (size $L_R \sim 19\,500 a_0$), using a mapped sine grid representation which involves a reasonable number of grid points. The time-dependent Schrödinger equation describing motion in two realistic potential curves coupled by the laser field is solved numerically.

At ultracold temperatures, the threshold effects which govern the dependence of the photoassociation rate as a function of the energy E have to be accounted for correctly. A high resolution analysis of such effects can be achieved by considering a large number of unity-normalized wavefunctions in the box, from which energy normalized functions are deduced. A proper estimate of the absolute value of the photoassociation rate has then been obtained from an incoherent average over a thermal distribution of the energy normalized wavefunctions;

– (ii) in the present paper, we have explored a large variety of pulses, all of them having the same central frequency, as described above, resonant with the level $v_0 = 98$. All of them have the same linear chirp parameter in the time domain, χ, designed so that after the pulse, at time $t_p + T_{vib}/2$ (where t_p corresponds to the maximum of the pulse, while T_{vib} is the classical vibrational period of v_0) the vibrational wavepacket created in the excited state is focussing at the inner turning point. This choice is dictated by the objective of improving the efficiency of the stabilization step, where either by spontaneous or by induced emission the population is transferred to bound levels of the $a^3\Sigma_u^+$ ground triplet state. This chirp rate can easily be deduced from the revival period, which can be defined provided the populated levels stay in a small energy range around v_0. All the pulses are obtained from a Gaussian transform-limited pulse, with the same peak intensity $I_L = 120$ kW/cm^2. They differ by the spectral width $\delta\omega \sim (\tau_L)^{-1}$. By varying τ_L from 1 to 6 and 12 ps, various situations are analyzed, with narrow ($\sim$1 cm^{-1}) or broad ($\sim$15 cm^{-1}) spectral width, long ($\tau_C \sim 580$ ps) or short ($\tau_C \sim 1$ ps) duration of the pulse stretched by chirping. Indeed, for a given choice of $\delta\omega$ and χ, two different pulses can be associated: the first one, with $(\tau_C/\tau_L) \approx 1$ is referred to as "almost no-chirped", the second one, with $(\tau_C/\tau_L) \gg 1$ as "really chirped". The resonance window $2\hbar|\chi|\tau_C$ explored by the instantaneous frequency during the time interval $[t_P - \tau_C, t_P + \tau_C]$ is larger in the second case. Different situations are then encountered with respect to the validity of the impulsive approximation, or of the adiabaticity of the population inversion.

The conclusion of our study is that the "really chirped" pulses seem generally to be more efficient. In fact, we have observed two qualitatively different dynamical situations, depending upon the energy range defined by $\hbar(\delta\omega + |\chi|\tau_C)$, i.e. by the spectral width and the width of the resonance window:

– under the condition $\hbar(\delta\omega + |\chi|\tau_C) < \delta_L^{at}$, already considered in previous work [20], the concept of a photoassociation window is relevant. In spite of the delocalized character of the initial wavefunction, we observe after the pulse a wavepacket in the excited state localized around R_L, with a finite extension $[R_{min}, R_{max}]$, corresponding to the domain of variation of the outer turning points of the vibrational levels in the photoassociation window. Indeed, whereas during the time window $[t_P - \tau_C, t_P + \tau_C]$ levels outside this window are significantly populated, it is possible to optimize the parameters of the pulse so that an adiabatic model is valid where no population remains, after the pulse, outside the photoassociation window. By varying the size of the photoassociation window, it is possible to optimize the number of photoassociated molecules, and this direction should be further explored in future work.
For fixed detuning and spectral width, an increase of the laser coupling W_L modifies the photoassociation dynamics. Having defined a parameter α such that adiabatic population transfer is taking place in the window $[-\alpha\tau_C, +\alpha\tau_C]$, we have shown that a larger intensity is increasing the time window, and therefore the width of the photoassociation window $[-\hbar\alpha|\chi|\tau_C, +\hbar\alpha|\chi|\tau_C]$, where total population inversion is taking place. Therefore, as expected, the photoassociation rate should be increased at large intensities. However, the dynamics outside the photoassociation window at large internuclear distances ($R > 200 a_0$) becomes less adiabatic. Rabi oscillations appear during the pulse, and levels outside the photoassociation window, may remain populated after the pulse;
– another situation occurs when $\hbar(\delta\omega + |\chi|\tau_C) > \delta_L^{at}$, since it is possible to transfer population to the continuum, or to highly excited vibrational levels in the excited potential $V_e(R)$. The results of the calculations indeed show evidence for population transfer at large internuclear distances. After the pulse, due to the attractive character of $V_e(R)$, with $-C_3/R^3$ asymptotic behaviour, the wavepacket created in the excited state is moving towards shorter distances R. For the uppermost levels, with an outer turning point located beyond $\sim 500 a_0$, the vibrational half period $T_{vib}/2$ becomes comparable to the radiative lifetime, so that spontaneous emission may take place before the intermediate distance region is reached, the photoassociated molecule decaying into a pair of atoms. In contrast, the wavepacket corresponding to lower levels has time to reach the intermediate region where

spontaneous or induced emission may populate bound levels in the V_g potential. The present calculations indicate that besides the acceleration due to the potential, the laser pulse has given a "kick" to the wavepacket in the V_e curve, thus reducing the time necessary to reach the intermediate distance region where radiative stabilization of the molecule may take place. Optimization of the pulses in view of increasing this "kick" is a promising direction for future work, since at large distances the continuum wavefunctions representing the initial state display a large amplitude, and many vibrational levels of the V_e potential are located close to dissociation limit, making the photoassociation process very efficient at small detunings, while it is well-known from cw experiments that the bottleneck in such situation is the stabilization process [1].

Future work should investigate photoassociation with better values for the detuning, since the present choice corresponds to a minimum in the cw photoassociation spectra.

Both the present paper and reference [20] have been investigating the population transferred to the excited state due to photoassociation with one chirped laser pulse. In order to get final conclusions more useful to experiments, the theoretical work should develop further in two directions. First, besides the photoassociation step, future calculations should investigate the efficiency of the stabilization process, bringing molecules to bound levels of the ground or lower triplet state, via spontaneous or induced emission. In particular the relevance of two-colour experiments where a second pulse with a larger central frequency is transferring population to the desired levels should be analyzed. Second, although the present estimation for photoassociation with a realistic repetition rate is promising, it does not take into account the fact that the second and further pulses are operating on a modified initial continuum state, where population has been extracted to be transferred to bound levels in the excited or ground state, or redistributed in the neighbouring continuum levels. The evolution of the atomic sample in the presence of a sequence of short pulses is an important issue, particularly in view of possible applications to condensates.

Some experiments on photoassociation of cold rubidium atoms have been started, making use of shorter pulses [48]. The pulses that we discuss here are designed for focussing the photoassociated wavepacket, and could be achieved experimentally [49]. Alternatively, calculations of photoassociation with shorter pulses will be developed, looking for different criteria in order to optimize the formation of stable molecules in the vibrational levels v_0 of the ground $a^3\Sigma_u^+$ triplet state, by introducing a second pulse to transfer population to low v_0 levels.

Many of the results obtained from the present analysis should be valid for similar systems: in particular, the possibility to convert easily all the pairs of atoms in a standard trap into molecules in a few tens of milliseconds make the use of chirped laser pulses very promising for future photoassociation experiments.

Discussions with Fabien Bretenaker, Anne Crubellier, Ronnie Kosloff, Ian Walmsley and Kai Willner are gratefully acknowledged. This work was performed in the framework of the European Research Training Network "Cold Molecules", funded by the European Commission under contract HPRN CT 2002 00290. M.V. acknowledges for two three-months post-doctoral stays in Orsay funded by this contract.

Appendix A: The energy normalization of the ground state continuum wavefunctions calculated in a box

The s-wave ground state continuum wavefunctions (normalized in the energy scale: $\langle \Psi_{g,E} | \Psi_{g,E'} \rangle = \delta(E - E')$) have the following asymptotic behaviour:

$$|\Psi_{g,E}(R)| = \sqrt{\frac{2\mu}{\pi\hbar^2}} \frac{\sin(k(R) + \eta_g)}{\sqrt{k(R)}} \tag{46}$$

where η_g is a slowly varying phase and $k(R)$ the local wave number determined by the electronic ground state potential $V_g(R)$: $k(R) = 1/\hbar\sqrt{2\mu(E - V_g(R))}$. For $E = E_n$, the energy-normalized wavefunction $\Psi_{g,E_n}(R)$ is deduced from the unity-normalized wavefunction $\phi_{g,E_n}(R)$ using the density of states $\partial E/\partial n \mid_{E=E_n}$ at the energy E_n [44,45]. Indeed, the classically allowed domain for a continuum wavefunction is $R_t \leq R \leq L_R$, where R_t is the inner turning point, and, in the standard semiclassical WKB form, the wavefunction can be written:

$$\Psi_{g,E=E_n}(R) = N_n \frac{1}{\sqrt{k(R)}} \sin\left(\int_{R_t}^{R} k(R')dR' + \frac{\pi}{4} \right) \tag{47}$$

with the Bohr-Sommerfeld quantization:

$$\int_{R_t}^{L_R} k(R')dR' = \left(n + \frac{1}{2} \right) \pi. \tag{48}$$

The normalization factor $(N_n)^{-2}$ is proportional to the density of states:

$$(N_n)^{-2} = \frac{2\mu}{\pi\hbar^2} \frac{\partial E}{\partial n} \mid_{E=E_n} = \frac{1}{2} \int_{R_t}^{L_R} \frac{dR'}{k(R')}. \tag{49}$$

Therefore:

$$\Psi_{g,E=E_n}(R) = \left[\frac{\partial E}{\partial n} \mid_{E=E_n} \right]^{-1/2} \phi_{g,E_n}(R). \tag{50}$$

Appendix B: Chirp rate in the time domain for focussing the excited vibrational wavepacket at the inner turning point

The Gaussian linearly chirped laser pulse excites successively several vibrational levels in the molecular surface V_e, creating a wavepacket located at the outer turning points

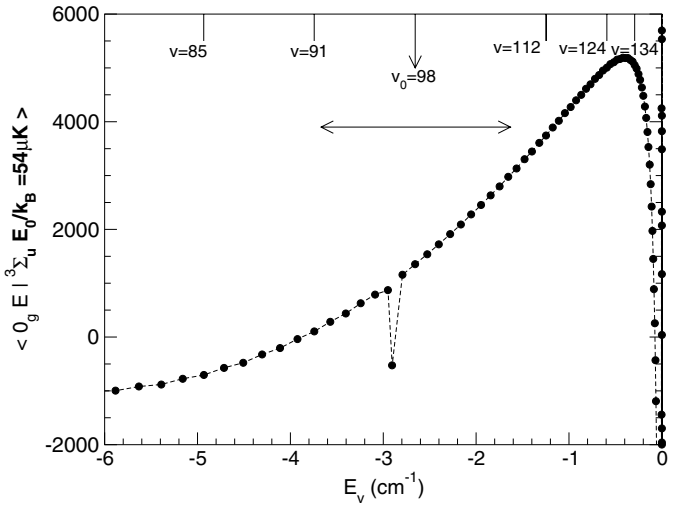

Fig. 12. The overlap between the initial stationary continuum state in the $a^3\Sigma_u^+$potential, corresponding to $E_0/k_B = 54$ μK, and the wavefunctions of the bound levels of the 0_g^- potential, with energies E_v between -6 and 0 cm^{-1} under the $6s+6p_{3/2}$ limit (the smaller value observed in the vicinity of -3 cm^{-1} is due to the tunneling from the outer well to the inner well of the 0_g^- potential). The horizontal arrow shows the "window" of 0_g^- vibrational levels between $v = 92$ and $v = 106$, excited by the pulse studied in reference [20].

of the corresponding vibrational wavefunctions. The center of the pulse excites at $t = t_P$ the level v_0. We choose the negative value of the chirp parameter $\chi < 0$ in the time domain such as the excited wavepacket, located initially at the outer turning points in the 0_g^- potential, to be focussed at the time $t = t_P + T_{vib}(v_0)/2$ at the inner turning points of the excited vibrational functions. Then the chirp value has to compensate the dispersion in the vibrational periods $T_{vib}(v)$ of the vibrational levels v resonantly excited at different times by the instantaneous frequency $\omega(t)/2\pi$ of the laser.

Let's note E_v the binding energy of the level v ($E_v > 0$, $\partial E_v/\partial v < 0$). The levels $v_0 + 1$, v_0 and $v_0 - 1$ are resonantly excited at $t_P - (E_{v_0+1} - E_{v_0})/(\hbar\chi) < t_P$, t_P, and $t_P - (E_{v_0-1} - E_{v_0})/(\hbar\chi) > t_P$, reaching their inner turning points with the delays $T_{vib}(v_0 + 1)/2$, $T_{vib}(v_0)/2$, and $T_{vib}(v_0 - 1)/2$, respectively. We deduce the value of the chirp χ from the condition that the components of the wavepacket should be in phase at the inner turning point. In a first approximation the χ is supplied by the condition:

$$\frac{T_{vib}(v_0)}{2} = -\frac{E_{v_0+1} - E_{v_0}}{\hbar\chi} + \frac{T_{vib}(v_0+1)}{2} = -\frac{E_{v_0-1} - E_{v_0}}{\hbar\chi} + \frac{T_{vib}(v_0-1)}{2}. \quad (51)$$

Using the definition of the vibrational period:

$$T_{vib}(v_0) = \frac{2\pi\hbar}{|\frac{\partial E}{\partial v}|_{v_0}|} \approx \frac{4\pi\hbar}{E_{v_0-1} - E_{v_0+1}}. \quad (52)$$

and of the revival period [47]:

$$T_{rev}(v_0) = \frac{4\pi\hbar}{|\frac{\partial^2 E}{\partial v^2}|_{v_0}|} \approx \frac{4\pi\hbar}{E_{v_0+1} + E_{v_0-1} - 2E_{v_0}}. \quad (53)$$

One can deduce the following value of χ from equations (51):

$$\chi = -2\pi\frac{T_{rev}(v_0)}{[T_{vib}(v_0)]^3}. \quad (54)$$

Appendix C: Overlap of the initial continuum with the 0_g^- vibrational wavefunctions

It is important, for qualitative discussions on the various domain of internuclear distances, to keep in mind the typical variation of overlap integrals between stationary wavefunctions. We have represented in Figure 12 the overlap integral $|\langle 0_g^-\ E_v|^3\Sigma_u^+\ E_0 = k_BT\rangle|$ between the initial collisional state in the $a^3\Sigma_u^+$ potential, corresponding to $E_0/k_B = 54$ μK, and the wavefunctions of the bound levels of the 0_g^- potential, with energies E_v between -6 and 0 cm^{-1} under the $6s + 6p_{3/2}$ limit.

References

1. F. Masnou-Seeuws, P. Pillet, Adv. At. Mol. Opt. Phys. **47**, 53 (2001)
2. J.D. Weinstein, R. de Carvalho, T. Guillet, B. Friedrich, J.M. Doyle, Nature **395**, 148 (1998)
3. H.L. Bethlem, G. Berden, G. Meijer, Phys. Rev. Lett. **83**, 1558 (1999)
4. H.L. Bethlem, F.M.H. Crompvoets, R.T. Jonqma, S.Y.T. van de Meerakker, G. Meijer, Phys. Rev. A **65**, 053416 (2002)
5. H.R. Thorsheim, J. Weiner, P.S. Julienne, Phys. Rev. Lett. **58**, 2420 (1987)
6. A. Fioretti, D. Comparat, A. Crubellier, O. Dulieu, F. Masnou-Seeuws, P. Pillet, Phys. Rev. Lett. **80**, 4402 (1998)
7. T. Takekoshi, B.M. Patterson, R.J. Knize, Phys. Rev. Lett. **81**, 5105 (1999)
8. A.N. Nikolov, E.E. Eyler, X.T. Wang, J. Li, H. Wang, W.C. Stwalley, Ph. Gould, Phys. Rev. Lett. **82**, 703 (1999)
9. A.N. Nikolov, J.R. Ensher, E.E. Eyler, H. Wang, W.C. Stwalley, Ph. Gould, Phys. Rev. Lett. **84**, 246 (2000)
10. C. Gabbanini, A. Fioretti, A. Lucchesini, S. Gozzini, M. Mazzoni, Phys. Rev. Lett. **84**, 2814 (2000)
11. A.J. Kerman, J.M. Sage, S. Sainis, T. Bergeman, D. DeMille, Phys. Rev. Lett. **92**, 033004 (2004)
12. C.P. Koch, J.P. Palao, R. Kosloff, F. Masnou-Seeuws, Phys. Rev. A **70**, 013402 (2004)
13. H.M.J.M. Boesten, C.C. Tsai, B.J. Verhaar, D.J. Heinzen, Phys. Rev. Lett. **77**, 5194 (1996)
14. S.D. Gensemmer, P.L. Gould, Phys. Rev. Lett. **80**, 457 (1998)
15. F. Fatemi, K.M. Jones, H. Wang, I. Walmsley, P.D. Lett, Phys. Rev. A **64**, 033421 (2001)
16. M. Mackhholm, A. Giusti-Suzor, F.H. Mies, Phys. Rev. A **50**, 5025 (1994)

17. A. Vardi, D. Abrashkevich, E. Frishman, M. Shapiro, J. Chem. Phys. **107**, 6166 (1997)
18. J. Vala, O. Dulieu, F. Masnou-Seeuws, P. Pillet, R. Kosloff, Phys. Rev. A **63**, 013412 (2000)
19. M. Vatasescu, O. Dulieu, R. Kosloff, F. Masnou-Seeuws, Phys. Rev. A **63**, 033407 (2001)
20. E. Luc-Koenig, R. Kosloff, F. Masnou-Seeuws, M. Vatasescu, Phys. Rev. A **70**, 033414 (2004)
21. J. Baum, R. Tycko, A. Pines, Phys. Rev. A **32**, 3435 (1985)
22. J.S. Melinger, A. Hariharan, S.R. Gandhi, W.S. Warren, J. Chem. Phys. **95**, 2210 (1991)
23. J.S. Melinger, S.R. Gandhi, A. Hariharan, J.X. Tull, W.S. Warren, Phys. Rev. Lett. **68**, 2000 (1992)
24. D. Goswami, Phys. Rep. **374**, 385 (2002)
25. J. Cao, Ch. J. Bardeen, K. Wilson, Phys. Rev. Lett. **80**, 1406 (1998)
26. J. Cao, Ch. J. Bardeen, K. Wilson, J. Chem. Phys. **113**, 1898 (2000)
27. R. Kosloff, Annu. Rev. Phys. Chem. **45**, 145 (1994)
28. R. Kosloff, Quantum Molecular Dynamics on Grids, in *Dynamics of Molecules and Chemical Reactions*, edited by R.E. Wyatt, J.Z. Zhang (Marcel Dekker, New York, 1996), pp. 185–230
29. V. Kokoouline, O. Dulieu, R. Kosloff, F. Masnou-Seeuws, J. Chem. Phys. **110**, 9865 (1999)
30. K. Willner, O. Dulieu, F. Masnou-Seeuws, J. Chem. Phys. **120**, 548 (2004)
31. U. Banin, A. Bartana, S. Ruhman, R. Kosloff, J. Chem. Phys. **101**, 8461 (1994)
32. C. Amiot, O. Dulieu, R. Gutteres, F. Masnou-Seeuws, Phys. Rev. A **66**, 052506 (2002)
33. Ph. Pellegrini, Ph.D. thesis, Université Paris-XI, Laboratoire Aimé Cotton, 2003
34. N. Spies, Ph.D. thesis, Fachbereich Chemie, Universität Kaiserslautern, 1989
35. M. Vatasescu, Ph.D. thesis, unpublished, Université Paris-XI, Laboratoire Aimé Cotton, 1999
36. P. Pillet, A. Crubellier, A. Bleton, O. Dulieu, P. Nosbaum, I. Mourachko, F. Masnou-Seeuws, J. Phys. B **30**, 2801 (1997)
37. G. Bruhat, *Thermodynamique* (Masson, Paris, 1962)
38. A.G. Borisov, J. Chem. Phys. **114**, 7770 (2001)
39. R. Heather, H. Metiu, J. Chem. Phys. **86**, 5009 (1987)
40. R. Kosloff, H. Tal-Ezer, Chem. Phys. Lett. **127**, 223 (1986)
41. W.E. Milne, Phys. Rev. A **35**, 863 (1930)
42. A. Messiah, *Mécanique Quantique* (Dunod, Paris, 1959), Vol. I
43. A. Crubellier, E. Luc-Koenig, P. Naidon, to be submitted
44. L.D. Landau, E.M. Lifshitz, *Quantum Mechanics (Nonrelativistic theory)* (Oxford Pergamon, 1977)
45. V.N. Ostrovsky, V. Kokoouline, E. Luc-Koenig, F. Masnou-Seeuws, J. Phys. B At. Mol. Opt. Phys. **34**, L27 (2001)
46. P. S. Julienne, J. Res. Natl. Inst. Stand. Technol. **101**, 487 (1996)
47. I.Sh. Averbukh, N.F. Perelman, Phys. Lett. A **139**, 449 (1989)
48. I.A. Walmsley, private communication
49. F. Bretenaker, private communication